CONTENTS

SUMMARY 1 1/A5

INTRODUCTION 1 1/A5

SYMBOLS 2 1/A6

ANALYSIS 6 1/A10

Incompressible Boundary-Layer Formulation 6 1/A10

Numerical Procedure 9 1/A13

Finite-difference equations 9 1/A13

Newton linearization of viscous term 10 1/A14

Solution of linearized difference equations 12 1/B2

Compressible Boundary-Layer Formulation 14 1/B4

RESULTS AND DISCUSSION 20 1/B10

Comparison With Experimental Data 20 1/B10

Results Obtained With $\bar{m}$-Method 21 1/B11

Similar solutions 21 1/B11

Laminar separation . . . . . 23 /1B13

Turbulent separation 23 1/B13

Viscous interaction 24 1/B14

CONCLUDING REMARKS 25 1/C1

APPENDIX A – COEFFICIENTS OF FINITE-DIFFERENCE EQUATIONS FOR δ^*-METHOD 27 1/C3

APPENDIX B – FINITE-DIFFERENCE EQUATIONS AND SOLUTION TECHNIQUE FOR $\bar{m}$-METHOD 30 1/C6

REFERENCES 36 1/C12

FIGURES 39 1/D1

Item 830-H-15
NAS 1.60:1208
OCT 1 1 1978
COMPLETED
ORIGINAL

NASA Technical Paper 1208

Inverse Boundary-Layer Theory and Comparison With Experiment

James E. Carter

SEPTEMBER 1978

NASA

56

Item 830-H-15 NAS 1.60:1208

NASA Technical Paper 1208

Inverse Boundary-Layer Theory and Comparison With Experiment

James E. Carter
Langley Research Center
Hampton, Virginia

National Aeronautics
and Space Administration

**Scientific and Technical
Information Office**

1978

Blank Page

SUMMARY

Two new inverse boundary-layer computational procedures, which permit nonsingular solutions at separation and reattachment, are presented. In the first technique, which is for incompressible flow, the displacement thickness is prescribed and the pressure is deduced implicitly along with the solution. Comparisons are made by using this procedure with the turbulent experimental data of Chu and Young, and excellent agreement is obtained. The purpose of the second technique is to obtain an inverse computational procedure for compressible separated flows that is nonsingular at separation. In this formulation, a perturbation mass flow is prescribed for the compressible boundary-layer equations and the pressure is deduced implicitly along with the solution. Laminar and turbulent computations made by using this technique are presented and are typical of separated flow. In both inverse procedures, finite-difference techniques are used along with Newton iteration. The present boundary-layer procedures can be used either in the inverse or direct (pressure prescribed) mode, depending on the boundary conditions; in either mode the solution procedure is no more complicated than conventional boundary-layer computations. Both inverse techniques presented herein appear to be well suited for complete viscous-inviscid interaction computations.

INTRODUCTION

In recent years, significant progress has been made in the solution of flow fields which contain regions of separated flow. Despite the diversity of approaches, which have been reported, there seems to be a clear distinction that most techniques are either based on the Navier-Stokes equations with relatively large computer costs or more approximate procedures in which the simultaneous solution of the boundary-layer and inviscid-flow equations is obtained. This latter approach is often referred to as interacting boundary-layer theory. In cases in which massive separation occurs, such as a stalled airfoil, it seems apparent that the solution of the Navier-Stokes equations must be used to obtain a detailed description of the flow field. In this case, the separated viscous region occupies a significant portion of the flow and thereby makes the inherent assumptions of interacting boundary-layer theory highly questionable. Alternately, there are many flows of interest in which, despite the presence of separation, the viscous flow is confined to a relatively thin layer adjacent to the body surface, thereby rendering the use of the Navier-Stokes equations unnecessary for most, if not all, of the flow field. In the present paper, a

technique is presented for obtaining approximate solutions for boundary layers in which the separated region is of a limited extent. Despite this simplifying feature, conventional or direct boundary-layer theory (pressure distribution prescribed) cannot be used without significant modification, such as that used in reference 1, because the boundary-layer solution is singular at separation.

In a recently developed boundary-layer theory, the displacement thickness is prescribed in the streamwise direction, thereby resulting in the calculation passing smoothly through the separation point. The surface pressure distribution is then deduced from the boundary-layer calculation. This idea of an inverse boundary-layer procedure to avoid the separation singularity was first presented in reference 2 and later was reformulated in reference 3. An alternate inverse boundary-layer procedure is to prescribe the skin-friction distribution as demonstrated in references 3 to 5 and others. However, the prescribed displacement-thickness technique is preferable when the simultaneous interaction of the boundary layer and inviscid flow is considered.

The purpose of the present paper is to give a new prescribed displacement-thickness procedure, which is considerably simpler than that given previously in reference 3. The new procedure is no more complicated than a direct boundary-layer calculation. This procedure is presented for incompressible flow, and comparisons are made with the turbulent experimental data presented in reference 6. With a few modifications, this method is then extended to compressible flow, and some sample calculations for laminar and turbulent separated flow are presented.

An axisymmetric version of the incompressible procedure has been successfully interacted with an inviscid program described in reference 7 in which the relaxation solution of the potential equation is obtained. Calculations for the low-speed separated flow over an axisymmetric boattail-sting juncture are discussed in reference 8.

SYMBOLS

$A_n, B_n, C_n, D_n, E_n, H_n, P_n, Q_n$ — coefficients in finite-difference equations

$A'_n, E'_n, H'_n, Q'_n, R'_n, S'_n$ — coefficients in recurrence equations

$\hat{c}_f$ — skin-friction coefficient

c_f — skin-friction coefficient multiplied by $\sqrt{R_\infty}$

f	transformed stream function
$\tilde{f}$	perturbation stream function in $\bar{m}$-method
F	nondimensional velocity ratio, u/u_e
h	$= \int_0^\infty (\theta - 1)\, d\bar{\eta}$
j	$= \begin{cases} 0 \text{ for two-dimensional flow} \\ 1 \text{ for axisymmetric flow} \end{cases}$
k	constant of proportionality used in similar form of equations for $\bar{m}$-method
K	ratio of two adjacent η-mesh increments
l	$= \frac{\rho\mu}{\rho_e \mu_e}$
L	reference length
$\bar{m}$	perturbation mass flow
M	Mach number
N	maximum number of points across boundary layer
N_{Pr}	Prandtl number
$N_{Pr,turb}$	turbulent Prandtl number
q	column iteration counter
r_B	body radius
R_∞	free-stream Reynolds number, $\frac{\rho_\infty U_\infty L}{\mu_\infty}$

T	nondimensional static temperature, $T_{O,\infty}$
u	velocity component parallel to surface divided by U_∞
U_∞	free-stream velocity
v	velocity component normal to surface divided by U_∞ and multiplied by $\sqrt{R_\infty}$
V	transformed normal-velocity component
x	coordinate along surface divided by L
y	coordinate along surface divided by L and multiplied by $\sqrt{R_\infty}$
α	$= (\gamma - 1)M_e^2$
β	pressure-gradient parameter for Levy-Lees formulation, $\frac{2\xi}{u_e}\frac{du_e}{d\xi}$
$\bar{\beta}$	pressure-gradient parameter for $\bar{m}$-method, $\frac{d(\ln u_e)}{d\xi}$
$\hat{\beta}$	pressure-gradient parameter for δ^*-method, $\delta^{*2}u_e\frac{du_e}{dx}$
γ	ratio of specific-heat coefficient
δ	transformed displacement thickness multiplied by $\sqrt{R_\infty}$
δ^*	displacement thickness, $\int_0^\infty \left(1 - \frac{\rho\mu}{\rho_e\mu_e}\right) dy$
$\hat{\delta}^*$	dimensional displacement thickness
$\delta F, \delta u, \delta\bar{\beta}, \delta\hat{\beta}, \delta\theta, \delta\hat{\psi}$	increments in dependent variable between two successive column iterations
Δx	grid spacing in x-coordinate
$\Delta\eta$	grid spacing in η-coordinate

$\Delta\bar{\eta}$ grid spacing in $\bar{\eta}$-coordinate

$\Delta\xi$ grid spacing in ξ-coordinate

ϵ eddy-viscosity coefficient

$\bar{\epsilon}$ $= 1 + \frac{\epsilon}{\mu}$

$\hat{\epsilon}$ $= 1 + \frac{\epsilon}{\mu} \frac{N_{Pr}}{N_{Pr,turb}}$

η transformed normal coordinate for δ^*-method

$\bar{\eta}$ transformed normal coordinate for $\bar{m}$-method

$\hat{\eta}$ transformed normal coordinate for Levy-Lees formulation

θ static-temperature ratio, T/T_e

μ molecular-viscosity coefficient

ξ transformed tangential coordinate

ρ density divided by ρ_∞

ψ nondimensional stream function

$\hat{\psi}$ perturbation stream function in δ^*-method

ω vorticity

Subscripts:

e edge of boundary layer

m,n indices for ξ- and η-coordinates, respectively

w wall

∞ free stream

ANALYSIS

Incompressible Boundary-Layer Formulation

The boundary-layer forms of the nondimensional continuity and x-momentum equations for incompressible flow are

$$\frac{\partial u}{\partial x} + \frac{\partial v}{\partial y} = 0 \tag{1}$$

and

$$u \frac{\partial u}{\partial x} + v \frac{\partial u}{\partial y} = u_e \frac{du_e}{dx} + \frac{\partial}{\partial y}\left(\bar{\epsilon} \frac{\partial u}{\partial y}\right) \tag{2}$$

The normal coordinate y and velocity v have been scaled in the usual manner by $\sqrt{R_\infty}$. For laminar flows, the quantity $\bar{\epsilon}$, which appears in equation (2), is set equal to unity, whereas for turbulent flow

$$\bar{\epsilon} = 1 + \frac{\epsilon}{\mu} \tag{3}$$

where ϵ/μ is the ratio of the eddy-viscosity coefficient to the molecular-viscosity coefficient. The eddy-viscosity coefficient is used to relate the Reynolds stress to the velocity gradient in the usual manner; thus

$$-\rho\overline{u'v'} = \epsilon \frac{\partial u}{\partial y} \tag{4}$$

In the present calculations, a two-layer eddy-viscosity formulation has been used and is discussed by Cebeci and Smith in reference 9. In the inner region the formulation is based on Prandtl's mixing length model along with the van Driest damping factor. In the outer region Clauser's velocity defect model is used along with Cebeci's low Reynolds number correction. This two-layer eddy-viscosity model has been successfully used for many attached-flow calculations with mild pressure gradients; for separated flow it serves only as an approximate model. The purpose of the present paper is to develop a

computational technique for separated turbulent flows: at a later time this method, when used to make computations for comparison with separated turbulent data, could conveniently be used to test new and improved turbulence models.

A key feature of the present inverse boundary-layer method as well as that given previously (ref. 3) is the elimination of the continuity equation by introducing the stream function

$$u = \frac{\partial \psi}{\partial y} \tag{5}$$

$$v = -\frac{\partial \psi}{\partial x} \tag{6}$$

The combination of equation (5) and the definition of displacement thickness δ^* gives the asymptotic value of the stream function at the boundary-layer edge

$$\psi \to u_e (y - \delta^*) \quad \text{as} \quad y \to \infty \tag{7}$$

As a result, a perturbation stream function $\hat{\psi}$ can be introduced as

$$\hat{\psi} \equiv \frac{1}{\sqrt{2x}} \left[\psi - u(y - \delta^*) \right] \tag{8}$$

such that $\hat{\psi} \to 0$ as $y \to \infty$. In this manner a boundary condition is imposed on the stream function at the outer edge provided that the displacement thickness is known. This condition replaces the usual outer boundary condition $u \to u_e$ as $y \to \infty$. If the perturbation stream function is introduced into the governing equations (1) and (2) and the normal coordinate is conveniently scaled by δ^* to give $\eta = y/\delta^*$, then the governing equations become

$$\frac{\partial \hat{\psi}}{\partial \eta} = \frac{\delta^*}{\sqrt{2x}} (1 - \eta) \frac{\partial u}{\partial \eta} \tag{9}$$

$$\delta^{*2} u \frac{\partial u}{\partial x} - \delta^* \frac{\partial}{\partial x} \left[\sqrt{2x}\, \hat{\psi} + (\eta - 1) u \delta^* \right] \frac{\partial u}{\partial \eta} = \hat{\beta} + \frac{\partial}{\partial \eta} \left(\bar{\epsilon} \frac{\partial u}{\partial \eta} \right) \tag{10}$$

where

$$\hat{\beta} \equiv \delta^{*2} u_e \frac{du_e}{dx} \tag{11}$$

These equations can be solved either in the usual direct mode with u_e given or in the inverse mode with δ^* prescribed and u_e and $\hat{\beta}$ unknown. In the direct mode δ^*, which appears in equations (9) to (11), is not the displacement thickness but is some given function of x, such as $\delta^* = \sqrt{2x}$. In the direct and inverse modes the boundary conditions are

$$\left.\begin{aligned} &u = \hat{\psi} = 0 \quad \text{at} \quad \eta = 0 \\ &\text{Direct:} \quad u \to u_e \quad \text{as} \quad \eta \to \infty \\ &\text{Inverse:} \quad \hat{\psi} \to 0 \quad \text{as} \quad \eta \to \infty \end{aligned}\right\} \tag{12}$$

In the inverse mode it is assumed that the y-derivatives vanish at the outer boundary; consequently, the x-momentum equation becomes

$$\delta^{*2} u \frac{\partial u}{\partial x} = \hat{\beta} \tag{13}$$

The discussion on the numerical scheme shows that the unknown pressure gradient $\hat{\beta}$ is deduced implicitly along with the solution for u and $\hat{\psi}$. Hereafter this formulation, combined with the numerical procedure described in the following section, is referred to as the δ^*-method.

In the previous δ^*-method presented in reference 3, the unknown pressure gradient was eliminated by differentiating the x-momentum equation with respect to y, thus introducing the vorticity transport equation. The present formulation is preferable because, not only can it be solved in either the direct or inverse mode, but it avoids the complication of having to solve for the unknown surface vorticity as was required in the previous formulation. Furthermore, the vorticity formulation introduces the second y-derivative of the eddy-viscosity coefficient, as shown in reference 10. This formulation was sometimes found to cause oscillations in the outer part of the boundary layer when the two-layer model described previously was used.

Numerical Procedure

The governing equations are solved by using the Crank-Nicolson finite-difference scheme with Newton linearization. In the reversed flow region the Reyhner and Flügge-Lotz (ref. 11) approximation

$$u \frac{\partial u}{\partial x} = 0 \quad \text{for} \quad u < 0 \tag{14}$$

is used to prevent instability while preserving the usual rapid forward-marching scheme used for the boundary-layer equations. In a previous paper, Carter and Wornom (ref. 12) showed that a similar approximation

$$u \frac{\partial \omega}{\partial x} = 0 \quad \text{for} \quad u < 0 \tag{15}$$

introduces negligible errors in the reversed flow region if the absolute value of the reversed flow velocity is less than approximately $0.10u_\infty$. Cebeci (ref. 13) repeated some of the calculations made by Carter and Wornom (ref. 12) and showed that the approximations given in equations (14) and (15) yield about the same result.

Finite-difference equations.- A variable grid is used across the boundary layer to account adequately for the two-layer structure of a turbulent velocity profile with as few grid points as possible. With n used to denote the grid-point index in the normal direction, the first and second derivatives are approximated by

$$\left.\frac{\partial u}{\partial \eta}\right|_n = \frac{u_{n+1} - u_{n-1}}{(1 + K)\,\Delta\eta_{n-1}} \tag{16}$$

and

$$\left.\frac{\partial}{\partial \eta}\left(\bar{\epsilon}\frac{\partial u}{\partial \eta}\right)\right|_n = \frac{2}{K(1 + K)\,\Delta\eta^2_{n-1}}\left[\bar{\epsilon}_{n+\frac{1}{2}}\,u_{n+1} - \left(\bar{\epsilon}_{n+\frac{1}{2}} + K\bar{\epsilon}_{n-\frac{1}{2}}\right)u_n + K\epsilon_{n-\frac{1}{2}}\,u_{n-1}\right] \tag{17}$$

where $\Delta\eta_{n-1} = \eta_n - \eta_{n-1}$ and the constant $K = \Delta\eta_n/\Delta\eta_{n-1}$, which is a variable grid that has been used by a number of investigators of turbulent boundary layers. The finite-difference forms of the governing boundary-layer equations were obtained by using the difference expressions given in equations (16) and (17) in conjunction with the Crank-Nicolson scheme. Newton linearization was used on the nonlinear terms to accelerate the convergence of the iterative solution made at each streamwise location. The linearized

finite-difference form of the stream function and x-momentum equations, given in equations (9) and (10), are written as

$$\delta\hat{\psi}_n - \delta\hat{\psi}_{n-1} + P_n\left(\delta u_n - \delta u_{n-1}\right) = Q_n \tag{18}$$

and

$$A_n\delta u_{n-1} + B_n\delta u_n + C_n\delta u_{n+1} + D_n\delta\hat{\psi}_n = E_n + H_n\delta\hat{\beta} \tag{19}$$

where δu, $\delta\hat{\psi}$, and $\delta\hat{\beta}$ (inverse mode) denote the change in the dependent variable at a given point between two successive column iterations; that is

$$\delta u_n = u_n^{q+1} - u_n^q \tag{20}$$

where q is the iteration index. The coefficients in equations (18) and (19), which are assumed known from the previous iteration, are given in appendix A.

The truncation error in equations (16) and (17) is $0\left[(1 - K)\,\Delta\eta_{n-1}\right]$; thus, the scheme is second-order accurate provided that $K = 1 + 0(\Delta\eta)$. Blottner (ref. 14) used the same finite-difference expressions and demonstrated numerically that they are second-order accurate. Blottner reports to have made these calculations for a fixed value of $K = 1.82$; however, it can be shown that this statement is in error, and the actual K used by Blottner depends on the number of points N used across the boundary layer and is given by

$$K = 1.82^{10/N} \tag{21}$$

Equation (21) reduces to

$$K = 1 + \frac{10}{N}\ln 1.82 \tag{22}$$

as $N \to \infty$ and thus shows that $K = 1 + 0(\Delta\eta)$, thereby resulting in a second-order accurate scheme.

Newton linearization of viscous term.- The number of column iterations in the turbulent calculations could be halved by using Newton linearization on the viscous term in the inner region. When the shear is positive in that region (the following procedure was used only in that case), the viscous term is written as

$$\frac{\partial}{\partial \eta}\left(\bar{\epsilon}\,\frac{\partial u}{\partial \eta}\right) = \frac{\partial}{\partial \eta}\left[\left(1 + c_1\,\frac{\partial u}{\partial \eta}\right)\frac{\partial u}{\partial \eta}\right] \tag{23}$$

where c_1 is assumed known. With the difference expression given in equation (17) and Newton linearization, the viscous term can be expressed as

$$\left.\frac{\partial}{\partial \eta}\left(\bar{\epsilon}\,\frac{\partial u}{\partial \eta}\right)\right|_n = \frac{2}{K(1+K)\,\Delta\eta^2_{n-1}}\left\{\left(2\bar{\epsilon}_{n+\frac{1}{2}} - 1\right)\delta u_{n+1} - \left[2\bar{\epsilon}_{n+\frac{1}{2}} - 1 + K\left(2\bar{\epsilon}_{n-\frac{1}{2}} - 1\right)\right]\right.$$

$$\times\,\delta u_n + K\left(2\bar{\epsilon}_{n-\frac{1}{2}} - 1\right)\delta u_{n-1} + \bar{\epsilon}_{n+\frac{1}{2}}\,u_{n+1} - \left(\bar{\epsilon}_{n+\frac{1}{2}} + K\bar{\epsilon}_{n-\frac{1}{2}}\right)u_n$$

$$\left. + K\bar{\epsilon}_{n-\frac{1}{2}}\,u_{n-1}\right\} \tag{24}$$

Comparison of equation (24) with the usual formulation, where Newton linearization is not used on the eddy-viscosity coefficient

$$\left.\frac{\partial}{\partial \eta}\left(\bar{\epsilon}\,\frac{\partial u}{\partial \eta}\right)\right|_n = \frac{2}{K(1+K)\,\Delta\eta^2_{n-1}}\left[\bar{\epsilon}_{n+\frac{1}{2}}\,\delta u_{n+1} - \left(\bar{\epsilon}_{n+\frac{1}{2}} + K\bar{\epsilon}_{n-\frac{1}{2}}\right)\delta u_n\right.$$

$$+ K\bar{\epsilon}_{n-\frac{1}{2}}\,\delta u_{n-1} + \bar{\epsilon}_{n+\frac{1}{2}}\,u_{n+1} - \left(\bar{\epsilon}_{n+\frac{1}{2}} + K\bar{\epsilon}_{n-\frac{1}{2}}\right)u_n$$

$$\left. + K\bar{\epsilon}_{n-\frac{1}{2}}\,u_{n-1}\right] \tag{25}$$

shows that Newton linearization of the viscous term adds only a slight complication. Keller and Cebeci (ref. 15) were the first to use Newton linearization on the boundary-layer equations; however, they did not use it on the turbulent viscous term. Nevertheless they claimed that their calculations converged quadratically; that is, the residuals decrease as

$$\delta u_n^{q+1} \approx \left(\delta u_n^q\right)^2 \tag{26}$$

with each subsequent iteration.

This convergence rate was observed only in the laminar calculations in the present study; even with the Newton linearization on the inner eddy-viscosity law, the present turbulent calculations did not converge quadratically. On the basis of the observations in the present paper, it is not clear how Keller and Cebeci (ref. 15) obtained quadratic convergence for their turbulent calculations.

Solution of linearized difference equations.- Repeated application of equations (18) and (19) across the boundary layer results in a system of block tridiagonal linear equations, which are solved by the recurrence relations

$$\delta u_n = E_n' - H_n' \delta\hat{\beta} - A_n' \delta u_{n+1} \tag{27}$$

and

$$\delta\hat{\psi}_n = Q_n' - S_n' \delta\hat{\beta} - R_n' \delta u_{n+1} \tag{28}$$

where

$$\left.\begin{aligned} E_n' &= \frac{E_n - A_n E_{n-1}' - D_n\left(Q_n + Q_{n-1}' + P_n E_{n-1}'\right)}{q_1} \\ H_n' &= -\frac{H_n + A_n H_{n-1}' + D_n\left(S_{n-1}' + P_n H_{n-1}'\right)}{q_1} \\ A_n' &= \frac{C_n}{q_1} \\ q_1 &= B_n - \left(A_n + D_n P_n\right) A_{n-1}' - D_n\left(R_{n-1}' + P_n\right) \end{aligned}\right\} \tag{29}$$

and

$$\left.\begin{aligned} Q'_n &= Q_n + Q'_{n-1} + P_n E'_{n-1} - E'_n q_2 \\ S'_n &= S'_{n-1} + P_n H'_{n-1} - H'_n q_2 \\ R'_n &= -A'_n q_2 \\ q_2 &= R'_{n-1} + P_n\left(1 + A'_{n-1}\right) \end{aligned}\right\} \tag{30}$$

The recurrence constants given in equations (29) and (30) are computed from the wall to the edge of the boundary layer. Since the surface boundary conditions are all homogeneous $\left(\text{i.e., } \delta u_1 = \delta\hat{\psi}_1 = 0\right)$, the recurrence constants are initialized at $n = 1$ by setting

$$E'_1 = H'_1 = A'_1 = Q'_1 = S'_1 = R'_1 = 0 \tag{31}$$

In the inverse case the perturbation in the edge velocity δu_N (where N denotes the grid point at the boundary-layer edge) and the perturbation in the pressure gradient $\delta\hat{\beta}$ are deduced at the edge of the boundary layer. These quantities are found from the simultaneous solution of the recurrence relations, which results in

$$\delta u_{N-1} = E'_{N-1} - H'_{N-1}\delta\hat{\beta} - A'_{N-1}\delta u_N \tag{32}$$

$$\delta\hat{\psi}_{N-1} = Q'_{N-1} - S'_{N-1}\delta\hat{\beta} - R'_{N-1}\delta u_N \tag{33}$$

and the finite-difference forms of equation (13) and equation (9), where the latter is evaluated at $n = N - 1/2$, gives

$$B_N\delta u_N = E_N + H_N\delta\hat{\beta} \tag{34}$$

and

$$-\delta\hat{\psi}_{N-1} + P_N\left(\delta u_N - \delta u_{N-1}\right) = Q_N \tag{35}$$

in which the boundary condition $\delta\hat{\psi}_N = 0$ has been imposed.

The solution of equations (32) to (35) results in

$$\delta u_N = \frac{Q_N + Q'_{N-1} + P_N E'_{N-1} + E_N\left(S'_{N-1} + P_N H'_{N-1}\right)}{R'_{N-1} + P_N\left(1 + A'_{N-1}\right) + B_N\left(S'_{N-1} + P_N H'_{N-1}\right)} \tag{36}$$

and then δu_{N-1}, $\delta\hat{\psi}_{N-1}$, and $\delta\hat{\beta}$ are deduced from equations (32) to (34). Now the back-substitution process is initiated, and the process continues down to the wall by using equations (27) and (28). Note that in this procedure the pressure gradient $\hat{\beta}$ is deduced simultaneously along with the boundary-layer solution u and $\hat{\psi}$. This procedure is similar to that developed previously by Reyhner (ref. 16). In a direct calculation, since u_e and $\hat{\beta}$ are known, $\delta u_N = \delta\hat{\beta} = 0$, and the back-substitution process begins by using equations (32) and (33). In either the direct or inverse calculation, the column iterative procedure is continued until

$$\max_n \left| \begin{pmatrix} \Delta u_n \\ \Delta\hat{\psi}_n \end{pmatrix} \right| \leq \epsilon_c \tag{37}$$

where ϵ_c is set equal to 10^{-4} in the present calculations. The number of column iterations typically required is 5.

Compressible Boundary-Layer Formulation

The compressible formulation is obtained by using a suitable compressibility transformation followed by an additional transformation to obtain an inverse formulation. These transformations could be considered together, but it is simpler to treat them separately. In the present study the Levy-Lees compressibility transformation (ref. 17), is used, although an analogous inverse formulation would have resulted if the Stewartson (ref. 18) transformation had been used. The nondimensional boundary-layer equations expressed after the Levy-Lees transformation (ref. 19) are given as follows:

Continuity:

$$2\xi\frac{\partial F}{\partial \xi} + F + \frac{\partial V}{\partial \hat{\eta}} = 0 \tag{38}$$

Momentum:

$$2\xi F \frac{\partial F}{\partial \xi} + V \frac{\partial F}{\partial \hat{\eta}} = \beta\left(\theta - F^2\right) + \frac{\partial}{\partial \hat{\eta}}\left(l\bar{\epsilon} \frac{\partial F}{\partial \hat{\eta}}\right) \tag{39}$$

Energy:

$$2\xi F \frac{\partial \theta}{\partial \xi} + V \frac{\partial \theta}{\partial \hat{\eta}} = \alpha l\bar{\epsilon}\left(\frac{\partial F}{\partial \hat{\eta}}\right)^2 + \frac{1}{N_{Pr}} \frac{\partial}{\partial \hat{\eta}}\left(l\hat{\epsilon} \frac{\partial \theta}{\partial \hat{\eta}}\right) \tag{40}$$

where the coordinates are transformed by

$$\xi = \int_0^x \rho_e u_e \mu_e r_B^{2j} \, dx \tag{41}$$

and

$$\hat{\eta} = \frac{\rho_e u_e r_B^j}{\sqrt{2\xi}} \int_0^y \frac{\rho}{\rho_e} \, dy \tag{42}$$

and the dependent variables are given by

$$\left.\begin{aligned} F &= \frac{u}{u_e} \\ \theta &= \frac{T}{T_e} \\ V &= \frac{2\xi}{\rho_e u_e \mu_e r_B^{2j}}\left(F \frac{\partial \hat{\eta}}{\partial x} + \frac{\rho v r_B^j}{\sqrt{2\xi}}\right) \end{aligned}\right\} \tag{43}$$

Additional quantities in equations (38) to (40) are given by

$$\left.\begin{aligned} l &= \frac{\rho\mu}{\rho_e \mu_e} \\ \alpha &= (\gamma - 1) M_e^2 \\ \beta &= \frac{2\xi}{u_e} \frac{du_e}{d\xi} \end{aligned}\right\} \tag{44}$$

The boundary conditions are given as follows:

Wall boundary:

$$\left.\begin{aligned} F(\xi,0) = V(\xi,0) &= 0 \\ \theta(\xi,0) &= \theta_w(\xi) \end{aligned}\right\} \quad \text{or} \quad \left.\frac{\partial\theta}{\partial\hat{\eta}}\right|_{\xi,0} = \left.\frac{\partial\theta}{\partial\hat{\eta}}\right|_{w}(\xi) \qquad (45)$$

Edge conditions:

$$F \text{ and } \theta \to 1 \text{ as } \hat{\eta} \to \infty \qquad (46)$$

The eddy-viscosity formulation used is the same as that in the δ^*-method. The turbulent Prandtl number enters the analysis in the compressible case in the term

$$\hat{\epsilon} = 1 + \frac{\epsilon}{\mu}\frac{N_{Pr}}{N_{Pr,turb}} \qquad (47)$$

where

$$N_{Pr,turb} = \frac{\overline{u'v'}(\partial T/\partial y)}{\overline{v'T'}(\partial u/\partial y)} \qquad (48)$$

Harris (ref. 19) presents a discussion of the turbulent Prandtl number; in the present analysis $N_{Pr,turb} = 0.95$.

The development of the inverse compressible formulation proceeds in an analogous manner to that developed previously for incompressible flow. A stream function f is introduced as

$$\frac{\partial f}{\partial\hat{\eta}} = F \qquad (49)$$

and the continuity equation is integrated to give

$$V = -\sqrt{2\xi}\,\frac{\partial}{\partial \xi}\left(\sqrt{2\xi}\, f\right) \tag{50}$$

where the boundary condition $V(\xi,0) = 0$ has been imposed. Introduction of a perturbation stream function is desired so that an outer boundary condition can be imposed from the prescribed displacement thickness. This boundary condition replaces the usual condition of β, the pressure gradient, being prescribed. The edge value of the stream function is

$$f_e = \int_0^\infty F\, d\hat{\eta} \tag{51}$$

The compressible displacement thickness is given by

$$\delta^* = \int \left(1 - \frac{\rho u}{\rho_e u_e}\right) dy \tag{52}$$

which becomes, after the Levy-Lees transformation

$$\delta^* = \frac{\sqrt{2\xi}}{\rho_e u_e r_B^j} \int_0^\infty (\theta - F)\, d\hat{\eta} \tag{53}$$

Combining equations (51) and (53) results in

$$f_e = \int_0^\infty \theta\, d\hat{\eta} - \frac{\rho_e u_e r_B^j \delta^*}{\sqrt{2\xi}} \tag{54}$$

A perturbation stream function is defined as

$$\tilde{f} = f - F\left(\int_0^\infty \theta\, d\hat{\eta} - \frac{\rho_e u_e r_B^j \delta^*}{\sqrt{2\xi}}\right) \tag{55}$$

such that the stream-function boundary conditions are

$$\tilde{f}(\xi,0) = \tilde{f}(\xi,\infty) = 0 \tag{56}$$

It is convenient to prescribe the perturbation mass flow

$$\bar{m} \equiv \rho_e u_e r_B^j \delta^* \tag{57}$$

instead of the displacement thickness because this grouping of quantities appears in the definition of the perturbation stream function. An inverse boundary-layer procedure based on mass flow instead of displacement thickness should be useful in a complete viscous-inviscid interaction since the effect of the boundary layer on the inviscid flow may be represented by imposing an injection (or suction) velocity at the solid surface given by

$$v_n = \frac{1}{\rho_e r_B^j} \frac{d\bar{m}}{dx} \tag{58}$$

It is also convenient to simplify the normal coordinate by introducing

$$\bar{\eta} = \frac{\sqrt{2\xi}}{\bar{m}} \hat{\eta} \tag{59}$$

which in terms of physical variables gives

$$\bar{\eta} = \frac{\int_0^y \frac{\rho}{\rho_e} dy}{\delta^*}$$

Note that $\bar{\eta}$ is the usual Dorodnitsyn variable (ref. 20) scaled by the displacement thickness. Use of this variable helps to reduce the effect of boundary-layer growth in the computation. With these definitions, the perturbation stream function becomes

$$\tilde{f} = f - \frac{F\bar{m}}{\sqrt{2\xi}} \left(\bar{\eta} - 1 + h \right) \tag{60}$$

where

$$h(\xi) \equiv \int_0^\infty (\theta - 1)\, d\bar{\eta}$$

The inverse compressible formulation is deduced from equations (38) to (40) by transforming from $\hat{\eta}$ to $\bar{\eta}$ and from V to $\tilde{f}$. The resulting system of equations is referred to as the prescribed perturbation mass-flow formulation and is given as

$$\frac{\partial \tilde{f}}{\partial \bar{\eta}} = \frac{\bar{m}}{\sqrt{2\xi}} (1 - \bar{\eta} - h) \frac{\partial F}{\partial \bar{\eta}} \tag{61}$$

$$\bar{m}^2 F \frac{\partial F}{\partial \xi} - \bar{m} \frac{\partial}{\partial \xi}\left[\sqrt{2\xi}\,\tilde{f} + \bar{m}F\left(\bar{\eta} - 1 + h\right)\right] \frac{\partial F}{\partial \bar{\eta}} = \bar{m}^2 \tilde{\beta}\left(\theta - F^2\right) + \frac{\partial}{\partial \bar{\eta}}\left(l\bar{\epsilon} \frac{\partial F}{\partial \bar{\eta}}\right) \tag{62}$$

and

$$\bar{m}^2 F \frac{\partial \theta}{\partial \xi} - \bar{m} \frac{\partial}{\partial \xi}\left[\sqrt{2\xi}\,\tilde{f} + \bar{m}F\left(\bar{\eta} - 1 + h\right)\right] \frac{\partial \theta}{\partial \bar{\eta}} = \alpha l\bar{\epsilon}\left(\frac{\partial F}{\partial \bar{\eta}}\right)^2 + \frac{1}{N_{Pr}} \frac{\partial}{\partial \bar{\eta}}\left(l\hat{\epsilon} \frac{\partial \theta}{\partial \bar{\eta}}\right) \tag{63}$$

These equations are solved for F, θ, $\tilde{f}$, and $\tilde{\beta} = \dfrac{d\left(\ln u_e\right)}{d\xi}$ for a prescribed streamwise distribution $\bar{m}$ subject to the following boundary conditions:

Wall boundary:

$$\left.\begin{aligned} &F(\xi,0) = \tilde{f}(\xi,0) = 0 \\ &\theta(\xi,0) = \theta_w(\xi) \\ &\text{or} \\ &\left.\frac{\partial \theta}{\partial \bar{\eta}}\right|_{\xi,0} = \left.\frac{\partial \theta}{\partial \bar{\eta}}\right|_w (\xi) \end{aligned}\right\} \tag{64}$$

Edge conditions:

$$F = \theta \to 1 \quad \text{and} \quad \tilde{f} \to 0 \quad \text{as} \quad \bar{\eta} \to \infty \tag{65}$$

Hereafter this formulation, combined with the numerical technique, which is now described, is referred to as the $\bar{m}$-method.

The Crank-Nicolson finite-difference scheme with Newton iteration is used to solve equations (61) to (63). The resulting finite-difference equations and solution technique are presented in appendix B since the technique is the same as that described previously. The energy equation is uncoupled from the combined stream function and x-momentum equations; as a result, quadratic convergence is not observed in the iterative convergence. At

a later time, when the present scheme is embodied in a complete viscous-inviscid interaction problem, it is planned to treat all three governing equations in a coupled manner by using Newton iteration. The resulting finite-difference equations will be a block tridiagonal system with each block being a 3×3 matrix provided that $h(\xi)$ is assumed to be known from the previous boundary-layer sweep.

RESULTS AND DISCUSSION

Comparison With Experimental Data

Chu and Young (ref. 6) reported an experiment in which measurements were made on a flat plate approximately $2\frac{1}{2}$ m long, which was first subjected to a favorable pressure gradient and then to an adverse pressure gradient. This pressure distribution was obtained by placing a 7.5-cm-diameter circular cylinder 11 cm above the flat plate with its axis parallel to the plate and normal to the windstream.

Calculations were made for this low-speed flow $\left(U_\infty = 18.7 \text{ m/s}\right)$ with the δ^* deduced by Chu and Young from velocity profile measurements prescribed in the streamwise direction. The δ^*-method is used instead of the incompressible version of the $\overline{m}$-method since, with the latter formulation, the computation is done in terms of a transformed x-coordinate

$$\xi = \int_0^x u_e \, dx \tag{66}$$

and requires $\overline{m} = u_e \delta^*$ to be prescribed as a function of ξ. Since u_e is unknown, it is preferable in the present application of inverse boundary-layer theory to use the δ^*-method which requires only $\delta^*(x)$ to be specified. Note that in a complete interaction calculation, in which an appropriate inviscid scheme is combined with the $\overline{m}$-method, repeated streamwise computations are made, and therefore the most recent distribution of u_e can be used to transform from the x-coordinate to the ξ-coordinate and conversely.

The upstream profile of u was obtained by using Coles' (ref. 21) wall-wake velocity distribution. This profile formulation contains three constants, which are determined by matching with experimental data. In the present case four quantities, δ^*, c_f, θ, and u_e, were known from Chu and Young's measurements. In order to use all the data to deduce the constants in Coles' formulation, a least-squares error calculation was used. Also, the wall-wake profile was modified near the surface by Kleinstein's formulation (ref. 22), thereby accounting for the laminar sublayer. At the outer edge of the boundary layer an exponential function was used to force the wall-wake profile for u to approach asymptotically u_e. After the u-profile was known, the perturbation stream function $\hat{\psi}$ was

deduced by integrating equation (9) from $\eta = 0$ where $\tilde{\psi}(\xi,0) = 0$. Ninety-three grid points were used across the boundary layer with $K = 1.09$.

A cubic spline fit to the displacement-thickness distribution measured by Chu and Young is shown in figure 1. This curve fit to the data was obtained by using a computer program developed by Smith and others (ref. 23) to represent the desired function by a cubic polynomial over prescribed intervals. Note that the displacement thickness shown in figure 1 is dimensional and is denoted as $\tilde{\delta}^*$. In order to demonstrate the capabilities of the present technique in separated flow, the prescribed $\tilde{\delta}^*$-distribution extends in figure 1 beyond the data of Chu and Young in a manner typical of a turbulent boundary layer incurring both separation and reattachment.

Figure 2 shows the comparison of the computed skin-friction coefficient on the flat plate with the experimental distribution obtained by Chu and Young. The agreement is good despite the use of an algebraic eddy-viscosity model, which is generally considered to be inappropriate for turbulent boundary layers subjected to large pressure gradients. Chu and Young also applied several direct boundary-layer procedures to these data and found that only the Bradshaw (ref. 24) and Kuhn and Nielsen (ref. 25) procedures gave good agreement with the data. None of these direct procedures can be used downstream of the separation point as exhibited by the present inverse calculation shown in figure 2. Figure 3 shows good agreement between the computed and measured velocity distribution at the edge of the boundary layer on the flat plate. Although more data are needed to assess the present method in a separated region, the good agreement shown in figures 2 and 3 between theory and experiment is encouraging and motivates the further use of inverse boundary-layer theory. The present comparison was simplified by the use of the experimental δ^*-distribution, thereby requiring only one streamwise boundary-layer calculation to be made. In a complete interaction calculation it is necessary to combine a suitable inviscid calculation with an inverse boundary-layer calculation and to solve the two simultaneously until convergence. A study demonstrating this technique for incompressible flow is reported in reference 8.

Results Obtained With $\overline{m}$-Method

Similar solutions.- A similar form of the mass-flow prescribed formulation is obtained by setting $\overline{m} = k\sqrt{2\xi}$, where k is a prescribed constant, and by assuming that $\frac{\partial}{\partial \xi} = 0$. The similar form of these equations for incompressible laminar flow is given by

$$\tilde{f}' = k(1 - \tilde{\eta})\, F' \tag{67}$$

and

$$-k\left[\tilde{f} + k(\bar{\eta} - 1)F\right]F' = k^2\beta\left(1 - F^2\right) + F'' \tag{68}$$

with the boundary conditions

$$\tilde{f}(0) = F(0) = 0 \tag{69}$$

and

$$\tilde{f} \to 0 \quad \text{and} \quad F \to 1 \quad \text{as} \quad \bar{\eta} \to \infty \tag{70}$$

where the prime denotes differentiation with respect to $\bar{\eta}$. A general, compressible, similar formulation cannot be obtained from the $\overline{m}$-method because the edge Mach number M_e appears explicitly in the energy equation. If $\beta \neq 0$, then $M_e = M_e(\xi)$, and thus the energy equation is not independent of ξ. A compressible similar formulation can be obtained by using the total-enthalpy form of the energy equation as was done by Cohen and Reshotko (ref. 26), thereby eliminating M_e from the equation when the Prandtl number is unity.

Incompressible similar solutions were obtained by solving equations (67) and (68) for different values of k subject to the boundary conditions given in equations (69) and (70). The prescribed constant k is easily shown to be equal to δ, where δ is the transformed displacement thickness expressed in terms of the Levy-Lees coordinate $\bar{\eta}$; thus

$$\delta = \int_0^\infty (1 - F)\, d\bar{\eta} \tag{71}$$

Results of these solutions are compared in figure 4 with so-called exact solutions, which previous investigators (e.g., see ref. 27) have obtained by numerical means. Excellent agreement is obtained. It is observed in figure 4 that for each value of β, the pressure-gradient parameter, there are two values for both the transformed displacement thickness δ and the wall shear F'_w. Thus, in a direct calculation, that is when β is prescribed, it is not clear what values of F'_w and δ will be obtained. Previously, unless a shooting technique was used, the forward flow solution $F'_w > 0$ and corresponding value of δ always resulted for a given value of β. Werle and Bertke (ref. 28) presented a double iterative procedure to obtain the reverse flow solutions $F'_w < 0$, which were originally discovered by Stewartson (ref. 29). In the present approach there was no difficulty in obtaining either the forward or reversed profile because figure 4(a) indicates that, given a value of δ, a single value of β results.

Laminar separation.- As a demonstration of the present procedure for computing separated boundary layers, the $\overline{m}$-distributions shown in figure 5(a) as a function of ξ were prescribed for both an incompressible and a compressible calculation. In the compressible case, $M_\infty = 2$ and the wall temperature was set equal to the free-stream stagnation temperature with $N_{Pr} = 1$. The two $\overline{m}$-distributions in figure 5(a) differ by a constant so that both $\overline{m}$-distributions match that of a flat-plate solution at $\xi = x = 1$. The initial boundary-layer profiles at this point were flat-plate similar solutions.

The resulting calculations for both cases are shown in figures 5(b), 5(c), and 5(d) for the edge velocity, skin friction, and displacement thickness, respectively. These quantities are plotted against the physical coordinate x, which is obtained after the calculation is completed from

$$x = \int_{\xi=0}^{\xi} \frac{d\xi}{\rho_e u_e \mu_e} \tag{72}$$

which for isentropic flow and a linear temperature-viscosity law becomes

$$x = \int_{\xi=0}^{\xi} \frac{d\xi}{u_e \left[1 + \frac{\gamma - 1}{2} M_\infty^2 \left(1 - u_e^2\right)\right]^{\gamma/(\gamma-1)}} \tag{73}$$

Although figures 5(b) to 5(d) show that the calculations for $M_\infty = 0$ and $M_\infty = 2$ differ in detail, the resulting solutions show the same basic features. This result is expected because equation (73) shows that if u_e remains close to unity (as shown in fig. 5(b)), then the physical and transformed streamwise coordinates are nearly the same, independent of the free-stream Mach number. Both solutions are smooth, and no difficulty was encountered near the separation or reattachment point in either solution. As a check on the computer program for the $\overline{m}$-method, the displacement thickness shown in figure 5(d) for the incompressible case was prescribed for the δ^*-method. The resulting solutions for u_e and c_f were identical to those shown in figures 5(b) and 5(c), respectively, for $M_\infty = 0$.

Turbulent separation.- A turbulent computation, similar to that shown for laminar flow, was made to demonstrate the present procedure for both an incompressible and compressible separated turbulent boundary layer. The prescribed $\overline{m}$-distributions are shown in figure 6(a) for the calculations with $M_\infty = 0$ and $M_\infty = 2$. As was the case for the laminar calculation, the prescribed $\overline{m}$-distributions match a turbulent flat-plate solution at the initial streamwise station $x = \xi = 0.95$ $\left(R_{\infty,x} = 0.95 \times 10^6\right)$. When this calculation was made the computer program using the $\overline{m}$-method had not been written so that

a direct calculation could be made. Hence, the initial boundary-layer profiles had to be obtained elsewhere. In the incompressible case the program for the δ^*-method was run in the direct mode with $\hat{\beta} = 0$, and the flow was assumed to be turbulent from the leading edge of the flat plate. For the compressible case the upstream profiles were obtained with the computer program reported in reference 30.

The resulting distributions of edge velocity, skin friction, and displacement thickness are plotted against the physical coordinate x in figures 6(b), 6(c), and 6(d), respectively. In both cases, flow separation and reattachment occurred, and no difficulty was encountered in obtaining a smooth solution. In contrast with the laminar case, the distributions of u_e shown in figure 6(b) differ significantly from unity, thereby resulting in different inverse transformations from the ξ-coordinate to the x-coordinate using equation (73).

In view of the different distributions of u_e, it is not surprising that large differences occur between the distributions of skin friction and displacement thickness for $M_\infty = 0$ and $M_\infty = 2$ shown in figures 6(c) and 6(d), respectively. A common feature is that both solutions show that the points of reattachment and maximum displacement thickness occur close to the point of minimum-edge velocity (maximum pressure). This trend has been observed in separated turbulent flow measurements, such as those of Alber and others in reference 31.

Viscous interaction.- With the development of the $\bar{m}$-method described in this paper, efforts should now be directed at the complete problem of viscous interaction. This inverse boundary-layer procedure, which to the author's knowledge is the only compressible, inverse, finite-difference procedure based essentially on displacement thickness, appears to be well suited for viscous interaction as shown by equation (58). As mentioned previously, a study has been completed using the δ^*-method on axisymmetric boattails and is reported in reference 8. The results and interaction scheme seem promising. Several compressible interaction calculations using inverse integral procedures have been reported in the literature, such as those by Kuhn and Nielsen (ref. 4) and Thiede (ref. 32). Integral techniques have the disadvantage that the shape of the velocity profile must be specified by the user, whereas the finite-difference calculation does not. Also, the present finite-difference inverse boundary-layer procedure should provide a good means to test various turbulence models for separated flow much more economically than can be done with solutions of the Navier-Stokes equations. Most of the current Navier-Stokes computations are forced to use relatively coarse grid spacing in the viscous region adjacent to the body region. In constrast, boundary-layer procedures provide complete resolution of the viscous region because the computation is confined entirely to the viscous region.

The present $\bar{m}$-method should be useful for separated flows with supersonic as well as subsonic edge conditions. The main motivation for the development of inverse

boundary-layer theory has been directed at subsonic separated flows to eliminate the singularity encountered at the separation point. Werle and Vatsa (ref. 33) developed a new supersonic viscous interaction technique, which was a major achievement because it converted the calculation from an ill-posed initial value problem to a well-posed boundary-value problem. The disadvantage of their procedure was that, unless a great deal of care was taken, a singularity was obtained at the point of separation. If the present $\overline{m}$-method were used, while retaining the interaction model of Werle and Vatsa, it is anticipated that a well-posed boundary-value problem would result with no singularity at the separation point.

CONCLUDING REMARKS

Two inverse boundary-layer formulations and solution techniques are presented for separated boundary-layer calculations. In the first technique, which is only for incompressible flow, the displacement thickness is prescribed; comparisons made with this method show good agreement with experimental low-speed turbulent data up to the point of separation. Further comparison with experimental data is needed to assess the accuracy of the present boundary-layer method in a region of separated flow. It is anticipated that the boundary-layer approximations are still valid provided that the separated region is not large but, based on the current literature, significant improvements are needed in the turbulence model for a separated region.

The second inverse technique presented in this paper is applicable to compressible flows and is based on a prescribed perturbation mass-flow distribution. A solution technique is presented for this formulation, and sample calculations are presented for laminar and turbulent incompressible and compressible flows. In all these calculations the solution passes smoothly through the points of separation and reattachment.

Both inverse procedures appear to be well suited for use in complete viscous-inviscid interactions because they are based primarily on the displacement thickness. The next step in the development of a complete viscous-inviscid interaction theory is to combine the compressible inverse procedure with an appropriately modified inviscid technique for subsonic or supersonic flows. This viscous-inviscid iteration technique can then be compared with experiment to test its accuracy as well as the simultaneous development of more sophisticated turbulence models. Interacting boundary-layer theory provides a more economical means by which different turbulence models for separated flows can be tested than current Navier-Stokes computations. Finite-difference procedures

should prove superior to integral techniques because the latter requires the specification of the shape of the velocity profile.

Langley Research Center
National Aeronautics and Space Administration
Hampton, VA 23665
July 19, 1978

APPENDIX A

COEFFICIENTS OF FINITE-DIFFERENCE EQUATIONS FOR δ^*-METHOD

The stream function and x-momentum equations, given by equations (9) and (10), are differenced about the points $\left(m,\ n - \frac{1}{2}\right)$ and $\left(m - \frac{1}{2},\ n\right)$, respectively, where m denotes the x-grid-point index and n denotes the η-grid-point index. The resulting finite-difference equations are given by equations (18) and (19) in which the following coefficients appear:

$$A_n = e - \frac{\bar{\epsilon}_{m,n-\frac{1}{2}}}{(1+K)\,\Delta\eta^2_{n-1}} \tag{A1}$$

$$B_n = 2au_{m,n} - fc_1 + \frac{\bar{\epsilon}_{m,n+\frac{1}{2}} + K\bar{\epsilon}_{m,n-\frac{1}{2}}}{K(1+K)\,\Delta\eta^2_{n-1}} \tag{A2}$$

$$C_n = -e - \frac{\bar{\epsilon}_{m,n+\frac{1}{2}}}{K(1+K)\,\Delta\eta^2_{n-1}} \tag{A3}$$

$$D_n = -b_1 f \tag{A4}$$

$$\begin{aligned} E_n = {} & \bar{\beta}_{m-\frac{1}{2}} + a\left(u^2_{m-1,n} - u^2_{m,n}\right) + ef \\ & + \frac{1}{K(1+K)\,\Delta\eta^2_{n-1}}\Bigg[\bar{\epsilon}_{m,n+\frac{1}{2}}u_{m,n+1} - \left(\bar{\epsilon}_{m,n+\frac{1}{2}} + K\bar{\epsilon}_{m,n-\frac{1}{2}}\right)u_{m,n} \\ & + K\bar{\epsilon}_{m,n-\frac{1}{2}}u_{m,n-1} + \bar{\epsilon}_{m-1,n+\frac{1}{2}}u_{m-1,n+1} - \left(\bar{\epsilon}_{m-1,n+\frac{1}{2}} + K\bar{\epsilon}_{m-1,n-\frac{1}{2}}\right)u_{m-1,n} \\ & + K\bar{\epsilon}_{m-1,n-\frac{1}{2}}u_{m-1,n-1}\Bigg] \end{aligned} \tag{A5}$$

APPENDIX A

$$H_n = 1 \tag{A6}$$

$$P_n = \left(\frac{\delta^*}{\sqrt{2x}}\right)_m \left(\eta_{n-\frac{1}{2}} - 1\right) \tag{A7}$$

$$Q_n = \hat{v}_{m,n-1} - \hat{v}_{m,n} - F_n\left(u_{m,n} - u_{m,n-1}\right) \tag{A8}$$

$$a = \frac{\delta^{*2}_{m-\frac{1}{2}}}{2\Delta x} \tag{A9}$$

$$b_1 = \frac{\delta^*_{m-\frac{1}{2}}}{2(1+K)\,\Delta\eta_{n-1}} \left(\frac{\sqrt{2x}}{\Delta x} + \frac{1}{2\sqrt{2x}}\right)_{m-\frac{1}{2}} \tag{A10}$$

$$b_2 = \frac{\delta^*_{m-\frac{1}{2}}}{2(1+K)\,\Delta\eta_{n-1}} \left(\frac{\sqrt{2x}}{\Delta x} - \frac{1}{2\sqrt{2x}}\right)_{m-\frac{1}{2}} \tag{A11}$$

$$c_1 = \frac{\delta^*_{m-\frac{1}{2}}\left(\eta_n - 1\right)}{2(1+K)\,\Delta\eta_{n-1}} \left(\frac{\delta^*}{\Delta x} + \frac{1}{2}\frac{d\delta^*}{dx}\right)_{m-\frac{1}{2}} \tag{A12}$$

$$c_2 = \frac{\delta^*_{m-\frac{1}{2}}\left(\eta_n - 1\right)}{2(1+K)\,\Delta\eta_{n-1}} \left(\frac{\delta^*}{\Delta x} - \frac{1}{2}\frac{d\delta^*}{dx}\right)_{m-\frac{1}{2}} \tag{A13}$$

$$e = b_1\hat{v}_{m,n} - b_2\hat{v}_{m-1,n} + c_1 u_{m,n} - c_2 u_{m-1,n} \tag{A14}$$

and

$$f = u_{m,n+1} - u_{m,n-1} + u_{m-1,n+1} - u_{m-1,n-1} \tag{A15}$$

APPENDIX A

Note that $\bar{\epsilon}_{n\pm\frac{1}{2}}$ is given by

$$\bar{\epsilon}_{n\pm\frac{1}{2}} = \frac{\bar{\epsilon}_n + \bar{\epsilon}_{n\pm1}}{2} \tag{A16}$$

APPENDIX B

FINITE-DIFFERENCE EQUATIONS AND SOLUTION TECHNIQUE FOR $\overline{m}$-METHOD

Application of the Crank-Nicolson scheme with a variable grid and with Newton iteration to equations (61) and (62) about the points $\left(m, n - \frac{1}{2}\right)$ and $\left(m - \frac{1}{2}, n\right)$, respectively, results in the following system of linearized finite-difference equations where the notation is the same as that used previously:

$$A_n \delta F_{n-1} + B_n \delta F_n + C_n \delta F_{n+1} + D_n \delta f_n = E_n + H_n \delta \overline{\beta} \tag{B1}$$

$$\delta \tilde{f}_n - \delta \tilde{f}_{n-1} + P_n \left(\delta F_n - \delta F_{n-1} \right) = Q_n \tag{B2}$$

where

$$A_n = e_1 - \frac{(\ell \bar{\tau})_{m,n-\frac{1}{2}}}{(1 + K)\, \Delta \bar{\eta}^2_{n-1}} \tag{B3}$$

$$B_n = 2a F_{m,n} - c_1 e_2 + \left(\overline{m}^2 \overline{\beta} \right)_{m-\frac{1}{2}} \left(\frac{F_{m,n} + F_{m-1,n}}{2} \right)$$

$$+ \frac{1}{K(1 + K)\, \Delta \bar{\eta}^2_{n-1}} \left[(\ell \bar{\tau})_{m,n+\frac{1}{2}} + K (\ell \bar{\tau})_{m,n-\frac{1}{2}} \right] \tag{B4}$$

$$C_n = -e_1 - \frac{(\ell \bar{\tau})_{m,n+\frac{1}{2}}}{K(1 + K)\, \Delta \bar{\eta}^2_{n-1}} \tag{B5}$$

$$D_n = -b_1 e_2 \tag{B6}$$

APPENDIX B

$$E_n = a\left(F^2_{m-1,n} - F^2_{m,n}\right) + e_1 e_2 + H_n \bar{\beta}_{n-\frac{1}{2}}$$

$$+ \frac{1}{K(1+K)\Delta\bar{\eta}^2_{n-1}}\left\{(l\bar{\epsilon})_{m,n+\frac{1}{2}} F_{m,n+1} - \left[(l\bar{\epsilon})_{m,n+\frac{1}{2}} + K(l\bar{\epsilon})_{m,n-\frac{1}{2}}\right] F_{m,n}\right.$$

$$+ K(l\bar{\epsilon})_{m,n-\frac{1}{2}} F_{m,n-1} + (l\bar{\epsilon})_{m-1,n+\frac{1}{2}} F_{m-1,n+1}$$

$$- \left[(l\bar{\epsilon})_{m-1,n+\frac{1}{2}} + K(l\bar{\epsilon})_{m-1,n-\frac{1}{2}}\right] F_{m-1,n}$$

$$\left. + K(l\bar{\epsilon})_{m-1,n-\frac{1}{2}} F_{m-1,n-1}\right\} \qquad \text{(B7)}$$

$$H_n = \bar{m}^2_{m-\frac{1}{2}}\left[\frac{\theta_{m,n} + \theta_{m-1,n}}{2} - \left(\frac{F_{m,n} + F_{m-1,n}}{2}\right)^2\right] \qquad \text{(B8)}$$

$$P_n = \left(\frac{\bar{m}}{\sqrt{2\xi}}\right)_m \left(\bar{\eta}_{n-\frac{1}{2}} - 1 + h_m\right) \qquad \text{(B9)}$$

$$Q_n = \tilde{f}_{m,n-1} - \tilde{f}_{m,n} + P_n\left(F_{m,n-1} - F_{m,n}\right) \qquad \text{(B10)}$$

The additional coefficients which appear in equations (B3) to (B10) are given by

$$a = \frac{\bar{m}^2_{m-\frac{1}{2}}}{2\Delta\xi} \qquad \text{(B11)}$$

APPENDIX B

$$b_1 = \frac{\bar{m}_{m-\frac{1}{2}}}{2(1+K)\,\Delta\bar{\eta}_{n-1}}\left(\frac{\sqrt{2\xi}}{\Delta\xi} + \frac{1}{2\sqrt{2\xi}}\right)_{m-\frac{1}{2}} \tag{B12}$$

$$b_2 = \frac{\bar{m}_{m-\frac{1}{2}}}{2(1+K)\,\Delta\bar{\eta}_{n-1}}\left(\frac{\sqrt{2\xi}}{\Delta\xi} - \frac{1}{2\sqrt{2\xi}}\right)_{m-\frac{1}{2}} \tag{B13}$$

$$c_1 = \frac{1}{2(K+1)\,\Delta\bar{\eta}_{n-1}\Delta\xi}\,\bar{m}_{m-\frac{1}{2}}\bar{m}_m\left(\bar{\eta}_n - 1 + h_m\right) \tag{B14}$$

$$c_2 = \frac{1}{2(K+1)\,\Delta\bar{\eta}_{n-1}\Delta\xi}\,\bar{m}_{m-\frac{1}{2}}\bar{m}_{m-1}\left(\bar{\eta}_n - 1 + h_{m-1}\right) \tag{B15}$$

$$e_1 = b_1\tilde{f}_{m,n} - b_2\tilde{f}_{m-1,n} + c_1 F_{m,n} - c_2 F_{m-1,n} \tag{B16}$$

$$e_2 = F_{m,n+1} - F_{m,n-1} + F_{m-1,n+1} - F_{m-1,n-1} \tag{B17}$$

In the present calculations for simplicity $\ell = \frac{\rho\mu}{\rho_e\mu_e} = 1$, which is an approximation frequently used by others. Also, Newton linearization of the eddy viscosity in the x-momentum equation was used in the same manner as described in the main text for the δ^*-method.

As in the δ^*-method equations (B1) and (B2) can be solved either in the inverse mode where $\bar{m}$ is prescribed and $\bar{\beta}$ is deduced or in the direct mode where $\bar{\beta}$ is prescribed. In the direct mode if $\bar{m} = \sqrt{2\xi}$, then $\bar{\eta} = \dot{\eta}$, $\bar{\beta} = \beta$, and the resulting formulation is the usual Levy-Lees boundary-layer formulation where the transformed normal-velocity component has been replaced by

$$V = -\sqrt{2\xi}\,\frac{\partial}{\partial\xi}\left\{\sqrt{2\xi}\left[\bar{f} + F(\bar{\eta} - 1 + h)\right]\right\} \tag{B18}$$

APPENDIX B

Equations (B1) and (B2) are solved by the same solution technique presented for the incompressible formulation in the main text. In the inverse case, $\delta\bar{\beta}$, δF_{N-1}, and $\delta\tilde{f}_{N-1}$ are deduced from the simultaneous solution of

$$\delta F_{N-1} = E'_{N-1} - H'_{N-1}\delta\bar{\beta} \tag{B19}$$

$$\delta\tilde{f}_{N-1} = Q'_{N-1} - S'_{N-1}\delta\bar{\beta} \tag{B20}$$

$$\delta\tilde{f}_{N-1} + P_N\delta F_{N-1} = -Q_N \tag{B21}$$

where the boundary conditions $\delta F_N = \delta\tilde{f}_N = 0$ have been applied. In the direct case equation (B21) is replaced by

$$\delta\tilde{f}_N - \delta\tilde{f}_{N-1} + P_N\delta F_{N-1} = Q_N \tag{B22}$$

and equations (B19), (B20), and (B22) are solved for δF_{N-1}, $\delta\tilde{f}_{N-1}$, and $\delta\tilde{f}_N$ with $\delta\bar{\beta} = 0$. The back-substitution procedure is then carried out from the boundary-layer edge to the surface.

After F and $\tilde{f}$ are updated by solving the x-momentum and stream-function equation, the linearized form of the energy equation is solved. The finite-difference form of this equation is given by

$$A_n\delta\theta_{n-1} + B_n\delta\theta_n + C_n\delta\theta_{n+1} = D_n \tag{B23}$$

where

$$A_n = e_1 - \frac{(\ell\tilde{f})_{m,n-\frac{1}{2}}}{N_{Pr}(1+K)\Delta\eta^2_{n-1}} \tag{B24}$$

$$B_n = a\left(F_{m,n} + F_{m-1,n}\right) + \frac{(\ell\tilde{f})_{m,n+\frac{1}{2}} + K(\ell\tilde{f})_{m,n-\frac{1}{2}}}{N_{Pr}K(1+K)\Delta\eta^2_{n-1}} \tag{B25}$$

APPENDIX B

$$C_n = -e_1 - \frac{(l\hat{e})_{m,n+\frac{1}{2}}}{N_{Pr}K(1+K)\Delta\eta^2_{n-1}} \tag{B26}$$

$$D_n = a\left(F_{m,n} + F_{m-1,n}\right)\left(\theta_{m-1,n} - \theta_{m,n}\right) + e_1\left(\theta_{m,n+1} - \theta_{m,n-1}\right.$$

$$\left. + \theta_{m-1,n+1} - \theta_{m-1,n-1}\right) + (l\alpha\hat{e})_{m-\frac{1}{2},n}\left(\frac{1}{2(1+K)\Delta\eta_{n-1}}\right)^2$$

$$\times\left[\left(F_{m,n+1} - F_{m,n-1}\right)^2 + \left(F_{m-1,n+1} - F_{m-1,n-1}\right)^2\right] + \frac{1}{N_{Pr}K(1+K)\Delta\eta^2_{n-1}}$$

$$\times\left\{(l\hat{e})_{m,n+\frac{1}{2}}\theta_{m,n+1} - \left[(l\hat{e})_{m,n+\frac{1}{2}} + K(l\hat{e})_{m,n-\frac{1}{2}}\right]\theta_{m,n} + K(l\hat{e})_{m,n-\frac{1}{2}}\theta_{m,n-1}\right.$$

$$+ (l\hat{e})_{m-1,n+\frac{1}{2}}\theta_{m-1,n+1} - \left[(l\hat{e})_{m-1,n+\frac{1}{2}} + K(l\hat{e})_{m-1,n-\frac{1}{2}}\right]\theta_{m-1,n}$$

$$\left. + K(l\hat{e})_{m-1,n-\frac{1}{2}}\theta_{m-1,n-1}\right\} \tag{B27}$$

The solution to the energy equation is given by

$$\delta\theta_n = D'_n - A'_n\delta\theta_{n-1} \tag{B28}$$

where

$$D'_n = \frac{D_n - C_nD'_{n+1}}{B_n - C_nA'_{n+1}} \tag{B29}$$

$$A'_n = \frac{A_n}{B_n - C_nA'_{n+1}} \tag{B30}$$

APPENDIX B

The constants D'_n and A'_n are evaluated from the outer boundary $n = N$ with $D'_N = A'_N = 0$ to the wall. If the wall is isothermal, then $\delta\theta_1 = 0$ and the solution for $\delta\theta_n$ is deduced from equation (B28). If the heat transfer $\partial\theta/\partial\bar{\eta}(\xi,0)$ is specified, then the finite-difference form of this Neumann condition is solved along with equation (B28) to deduce $\delta\theta_1$. Then the back-substitution process given in equation (B28) begins.

REFERENCES

1. Bauer, Frances; Garabedian, Paul; Korn, David; and Jameson, Antony: Supercritical Wing Sections II. Volume 108 of Lecture Notes in Economics and Mathematical Systems, Springer-Verlag, 1975.

2. Catherall, D.; and Mangler, K. W.: The Integration of the Two-Dimensional Laminar Boundary-Layer Equations Past the Point of Vanishing Skin Friction. J. Fluid Mech., vol. 26, pt. 1, Sept. 1966, pp. 163-182.

3. Carter, James E.: Inverse Solutions for Laminar Boundary-Layer Flows With Separation and Reattachment. NASA TR R-447, 1975.

4. Kuhn, Gary D.; and Nielsen, Jack N.: Prediction of Turbulent Separated Boundary Layers. AIAA Paper No. 73-663, July 1973.

5. Klineberg, John M.; and Steger, Joseph L.: On Laminar Boundary-layer Separation. AIAA Paper No. 74-94, Jan.-Feb. 1974.

6. Chu, J.; and Young, A. D.: Measurements in Separating Two Dimensional Turbulent Boundary Layers. Flow Separation, AGARD-CP-168, Nov. 1975, pp. 13-1 - 13-12.

7. Keller, James D.; and South, Jerry C., Jr.: RAXBOD: A Fortran Program for Inviscid Transonic Flow Over Axisymmetric Bodies. NASA TM X-72831, 1976.

8. Carter, James E.: A New Boundary-Layer Interaction Technique for Separated Flows. NASA TM-78690, 1978.

9. Cebeci, Tuncer; and Smith, A. M. O.: Analysis of Turbulent Boundary Layers. Academic Press, Inc., 1974.

10. Carter, James E.; and Wornom, Stephen F.: Solutions for Incompressible Separated Boundary Layers Including Viscous-Inviscid Interaction. Aerodynamic Analyses Requiring Advanced Computers – Part I. NASA SP-347, 1975, pp. 125-150.

11. Reyhner, T. A.; and Flügge-Lotz, I.: The Interaction of a Shock Wave With a Laminar Boundary Layer. Int. J. Non-Linear Mech., vol. 3, no. 2, June 1968, pp. 173-199.

12. Carter, James E.; and Wornom, Stephen F.: Forward Marching Procedure for Separated Boundary-Layer Flows. AIAA J., vol. 13, no. 8, Aug. 1975, pp. 1101-1103.

13. Cebeci, Tuncer: Separated Flows and Their Representation by Boundary-Layer Equations. Report ONR-CR215-234-2, U.S. Navy, Sept. 1976. (Available from DDC as AD A035 693.)

14. Blottner, F. G.: Variable Grid Scheme Applied to Turbulent Boundary Layers. Comput. Methods Appl. Mech. & Eng., vol. 4, no. 2, Sept. 1974, pp. 179-194.

15. Keller, Herbert B.; and Cebeci, Tuncer: Accurate Numerical Methods for Boundary-Layer Flows. II: Two-Dimensional Turbulent Flows. AIAA J., vol. 10, no. 9, Sept. 1972, pp. 1193-1199.

16. Reyhner, Theodore Alison: The Interaction of a Shock Wave With a Laminar Boundary Layer. Ph. D. Diss., Stanford Univ., 1967.

17. Lees, Lester: Laminar Heat Transfer Over Blunt-Nosed Bodies at Hypersonic Flight Speeds. Jet Propul., vol. 26, no. 4, Apr. 1956, pp. 259-269, 274.

18. Stewartson, K.: Correlated Incompressible and Compressible Boundary Layers. Proc. R. Soc. (London), ser. A, vol. 200, no. A1060, Dec. 22, 1949, pp. 84-100.

19. Harris, Julius E.: Numerical Solution of the Equations for Compressible Laminar, Transitional, and Turbulent Boundary Layers and Comparisons With Experimental Data. NASA TR R-368, 1971.

20. Stewartson, K.: The Theory of Laminar Boundary Layers in Compressible Fluids. Oxford Univ. Press, Inc., 1964.

21. Coles, D.: The Law of the Wake in the Turbulent Boundary Layer. J. Fluid Mech., vol. 1, pt. 2, July 1956, pp. 191-226.

22. Kleinstein, Gdalia: Generalized Law of the Wall and Eddy Viscosity Model for Wall Boundary Layers. AIAA J., vol. 5, no. 8, Aug. 1967, pp. 1402-1407.

23. Smith, Robert E., Jr.; Price, Joseph M.; and Howser, Lona M.: A Smoothing Algorithm Using Cubic Spline Functions. NASA TN D-7397, 1974.

24. Bradshaw, P.; Ferriss, D. H.; and Atwell, N. P.: Calculation of Boundary Layer Development Using the Turbulent Energy Equation. J. Fluid Mech., vol. 28, pt. 3, May 26, 1967, pp. 593-616.

25. Kuhn, Gary D.; and Nielsen, Jack N.: An Analytical Method for Calculating Turbulent Separated Flows Due to Adverse Pressure Gradients. Tech. Rep. NEAR-1-PU, U.S. Navy Project Squid, Oct. 1971. (Available from DDC as AD 731 744.)

26. Cohen, Clarence B.; and Reshotko, Eli: Similar Solutions for the Compressible Laminar Boundary Layer With Heat Transfer and Pressure Gradient. NACA Rep. 1293, 1956. (Supersedes NACA TN 3325.)

27. Christian, James W.; Hankey, Wilbur L.; and Petty, James S.: Similar Solutions of the Attached and Separated Compressible Laminar Boundary Layer With Heat Transfer and Pressure Gradient. ARL 70-0023, U.S. Air Force, Feb. 1970. (Available from DDC as AD 705 581.)

28. Werle, M. J.; and Bertke, S. D.: A Finite-Difference Method for Boundary Layers With Reverse Flow. AIAA J., vol. 10, no. 9, Sept. 1972, pp. 1250-1252.

29. Stewartson, K.: Further Solutions of the Falkner-Skan Equation. Proc. Cambridge Philos. Soc., vol. 50, pt. 3, July 1954, pp. 454-465.

30. Anderson, E. C.; and Lewis, C. H.: Laminar or Turbulent Boundary-Layer Flows of Perfect Gases or Reacting Gas Mixtures in Chemical Equilibrium. NASA CR-1893, 1971.

31. Alber, Irwin E.; Bacon, John W.; Masson, Bruce S.; and Collins, Donald J.: An Experimental Investigation of Turbulent Transonic Viscous-Inviscid Interactions. AIAA J., vol. 11, no. 5, May 1973, pp. 620-627.

32. Thiede, P. G.: Prediction Method for Steady Aerodynamic Loading on Airfoils With Separated Transonic Flow. Prediction of Aerodynamic Loading, AGARD CP-204, Feb. 1977, pp. 16-1 - 16-12.

33. Werle, M. J.; and Vatsa, V. N.: New Method for Supersonic Boundary-Layer Separation. AIAA J., vol. 12, no. 11, Nov. 1974, pp. 1491-1497.

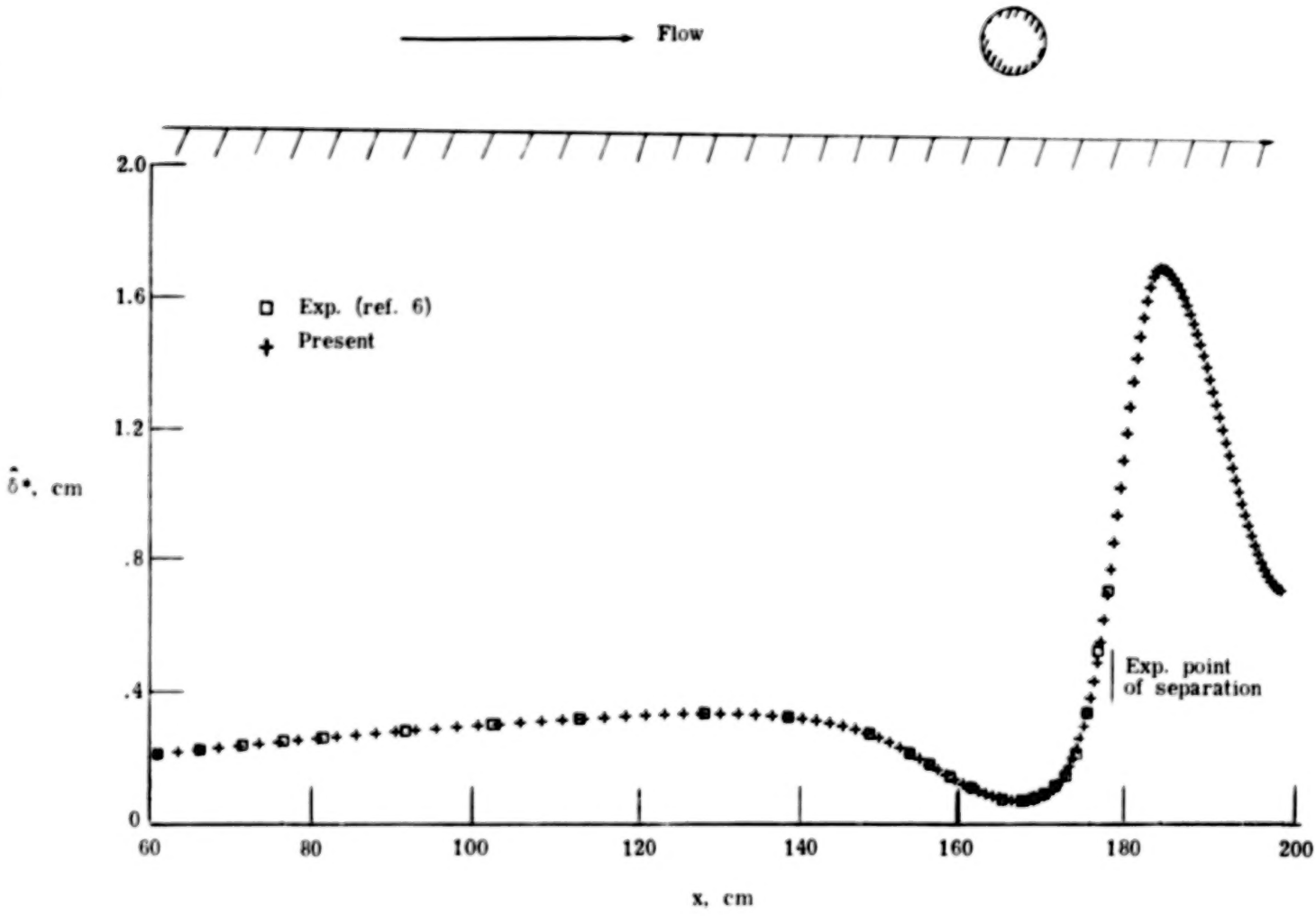

Figure 1.- Prescribed displacement-thickness distribution. $R_\infty = 2.08 \times 10^6$; $U_\infty = 18.7$ m/s.

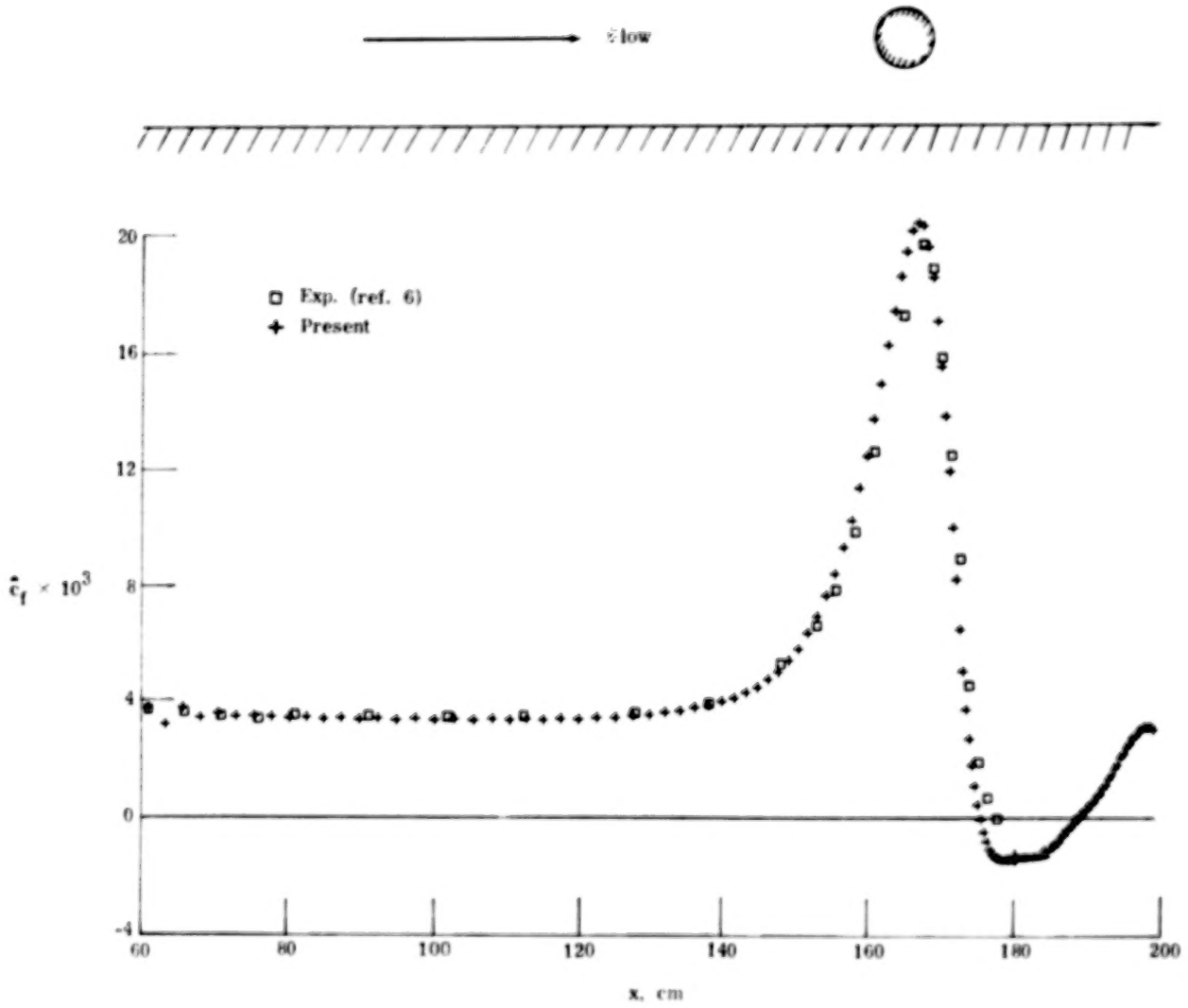

Figure 2.- Skin-friction distributions. $R_\infty = 2.08 \times 10^6$; $U_\infty = 18.7$ m/s.

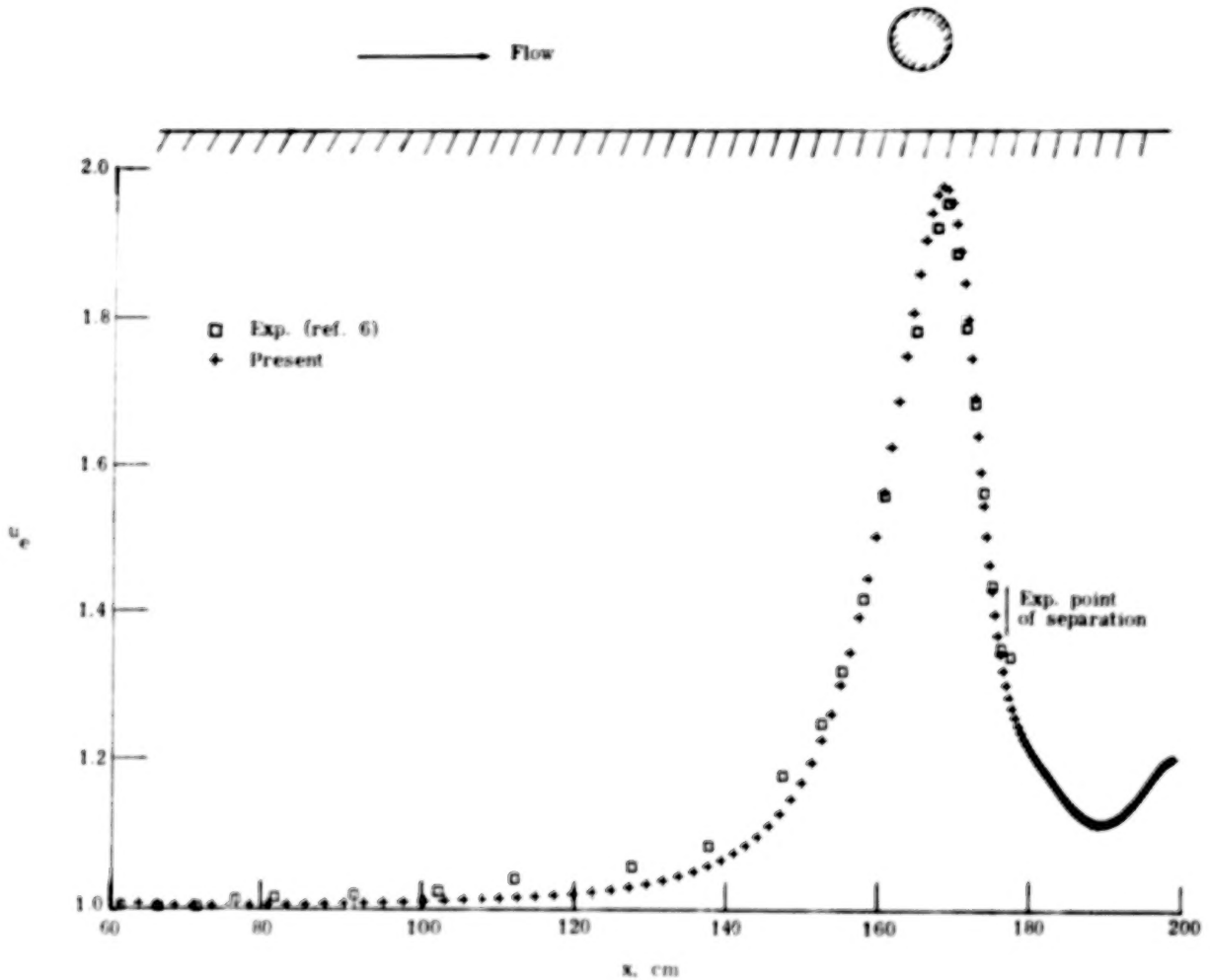

Figure 3.- Edge-velocity distributions. $R_\infty = 2.08 \times 10^6$; $U_\infty = 18.7$ m/s.

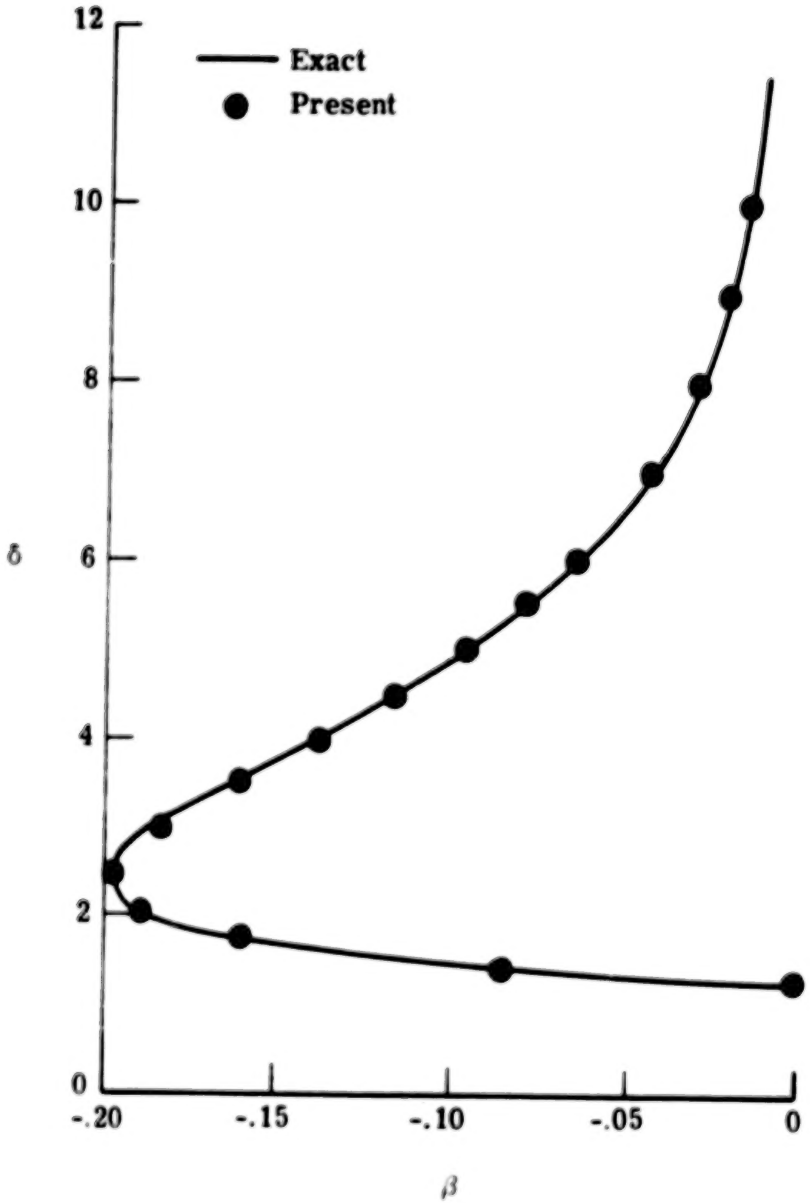

(a) Displacement thickness plotted against pressure gradient.

Figure 4.- Incompressible similar solutions.

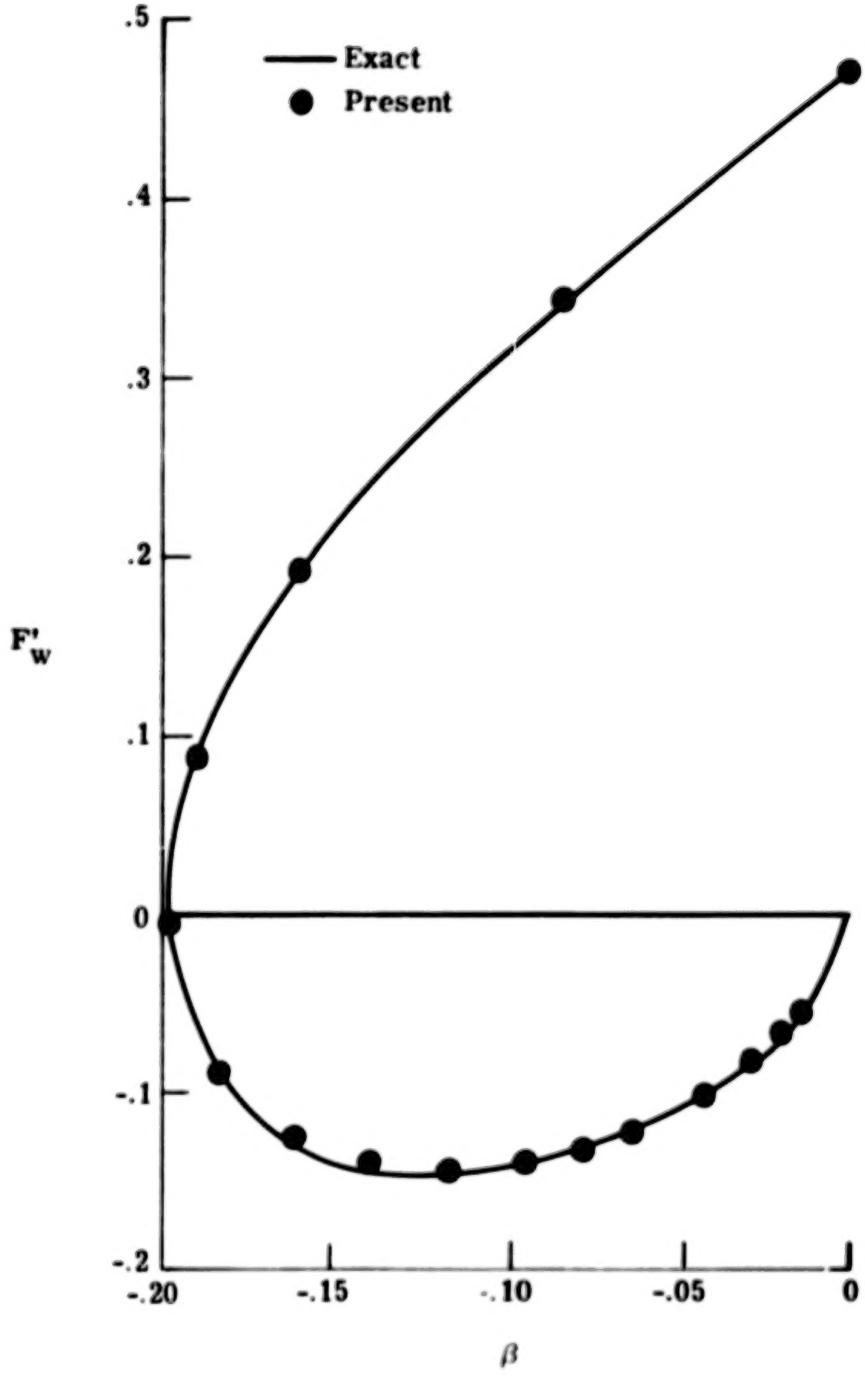

(b) Wall shear plotted against pressure gradient.

Figure 4.- Concluded.

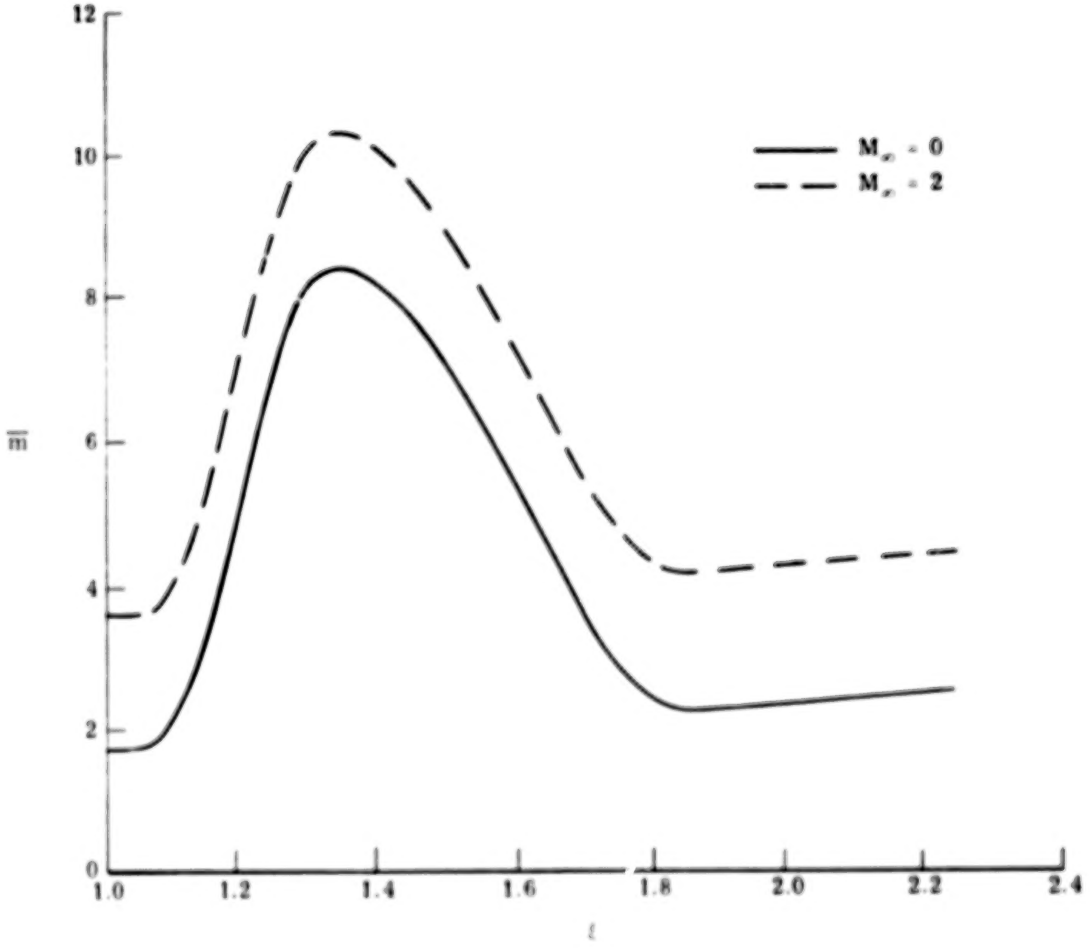

(a) Prescribed perturbation mass-flow distributions.

Figure 5.- Laminar-separation computations for $T_W = T_{O,\infty}$.

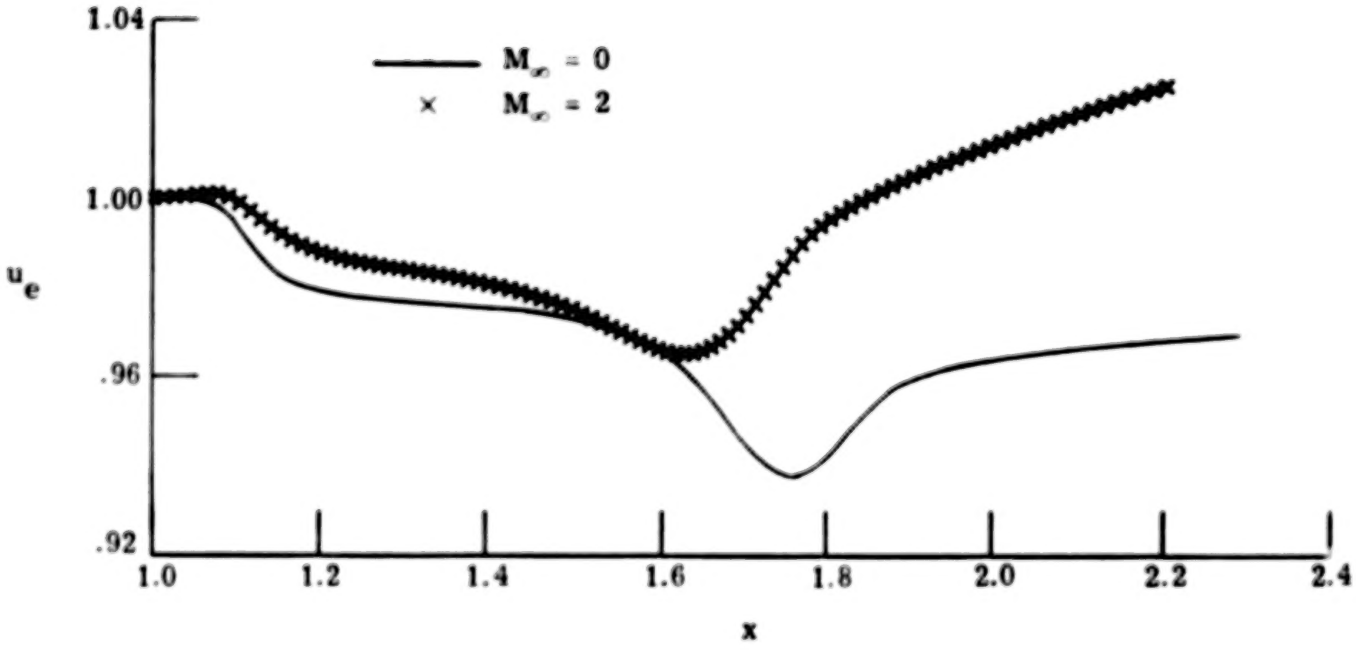

(b) Computed edge-velocity distributions.

Figure 5.- Continued.

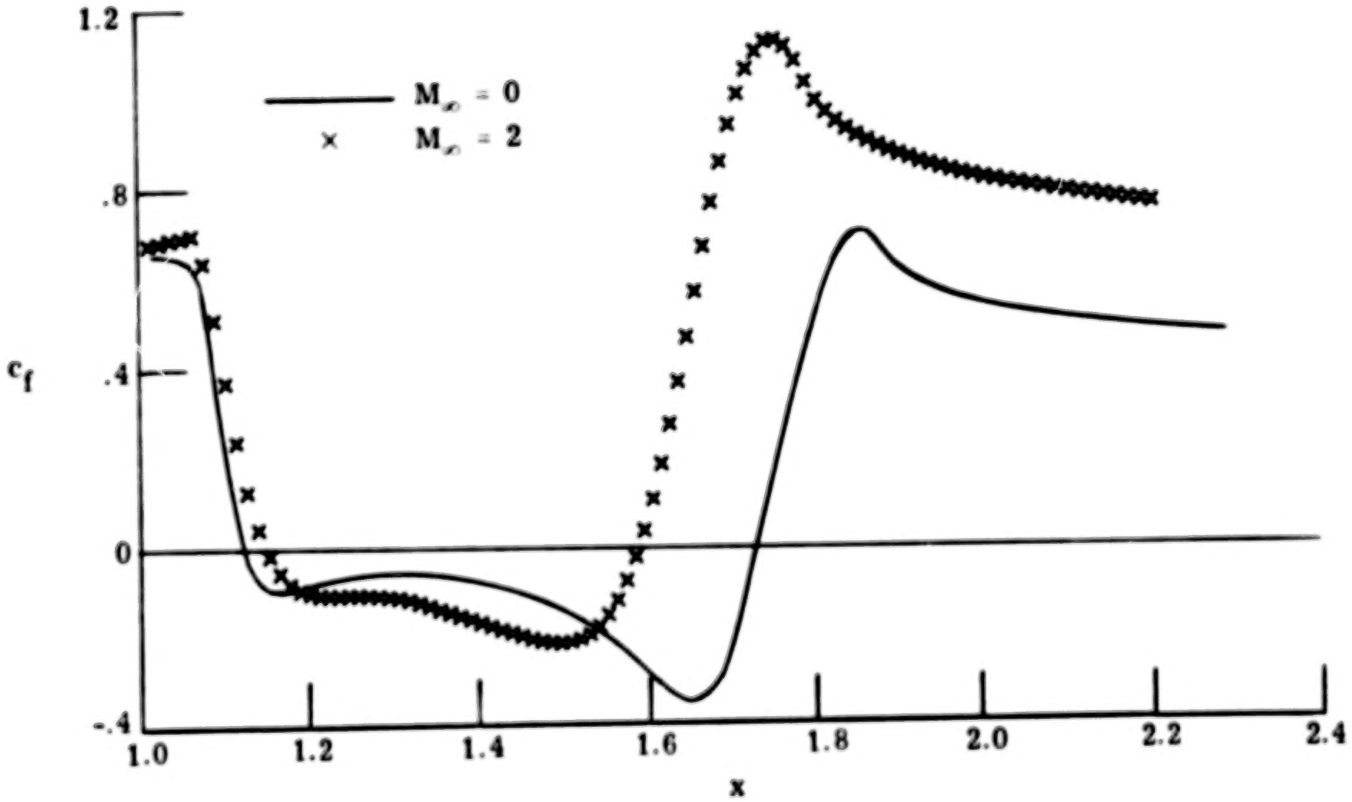

(c) Computed skin-friction distributions.

Figure 5.- Continued.

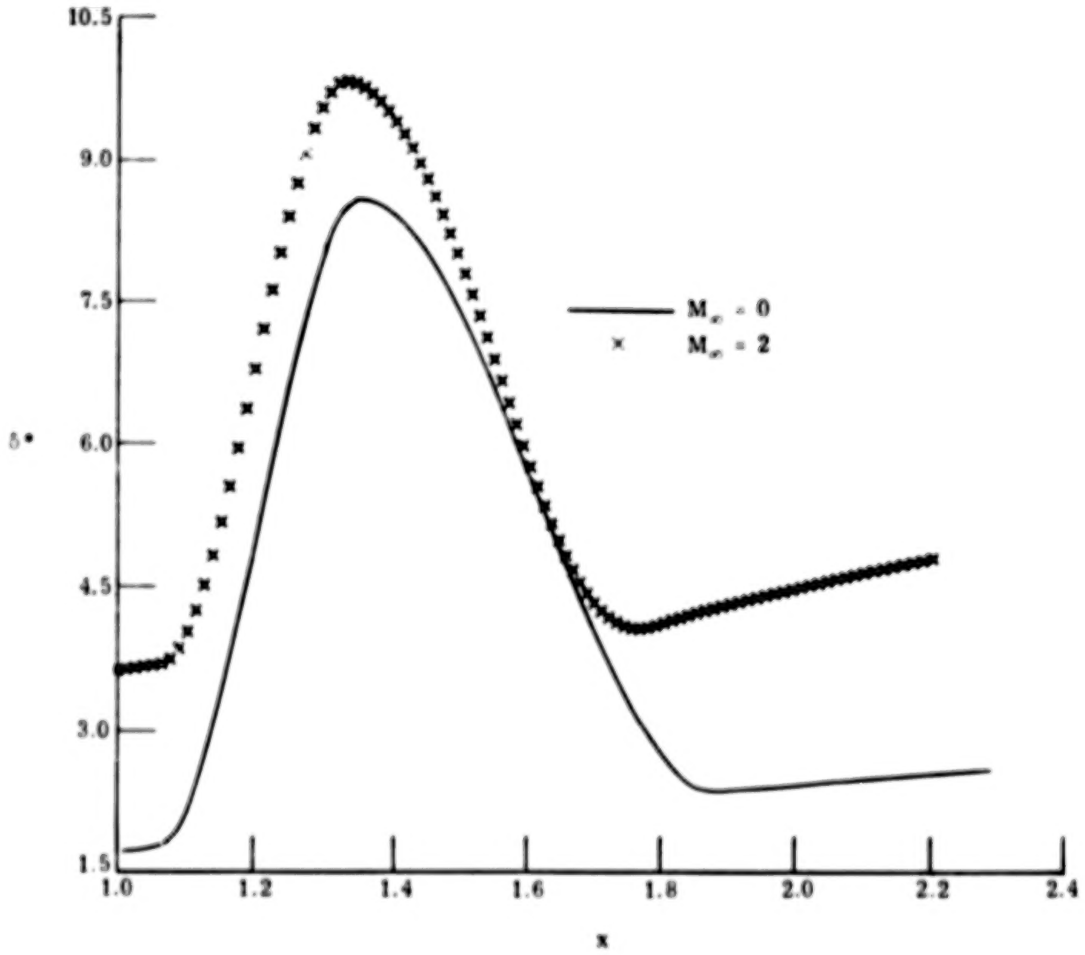

(d) Computed displacement-thickness distributions.

Figure 5.- Concluded.

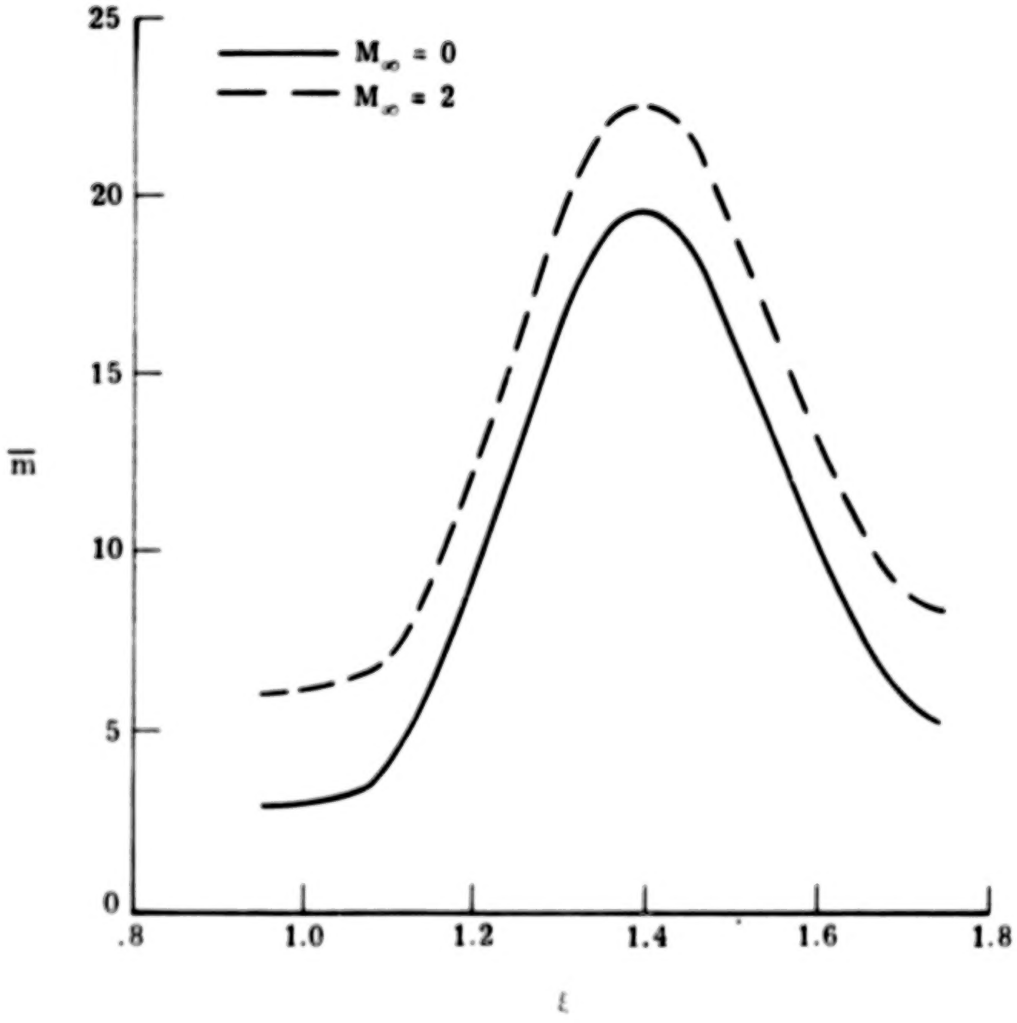

(a) Prescribed perturbation mass-flow distributions.

Figure 6.- Turbulent separation computations for $T_w = T_{0,\infty}$ and $R_\infty = 10^6$.

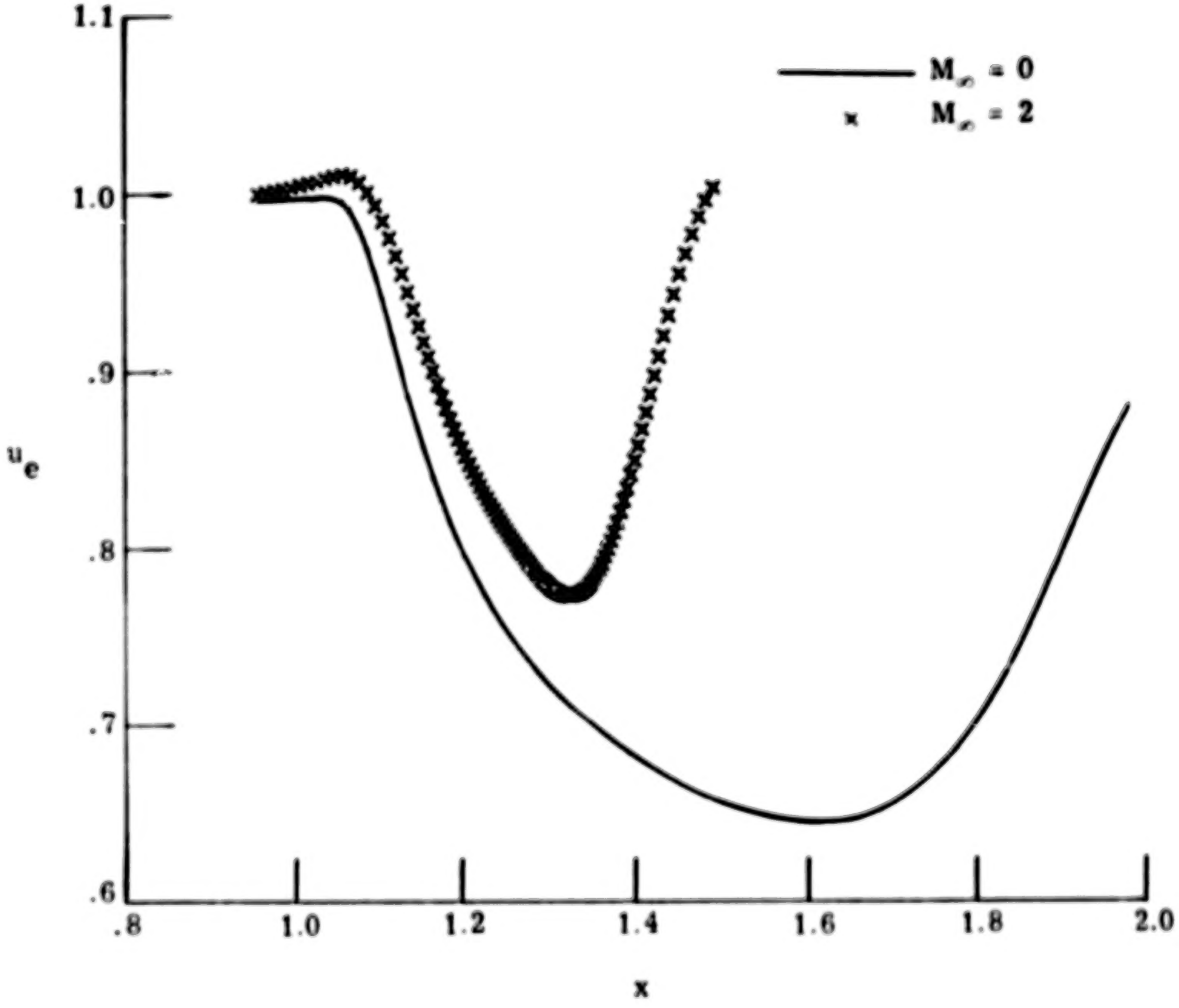

(b) Computed edge-velocity distributions.

Figure 6.- Continued.

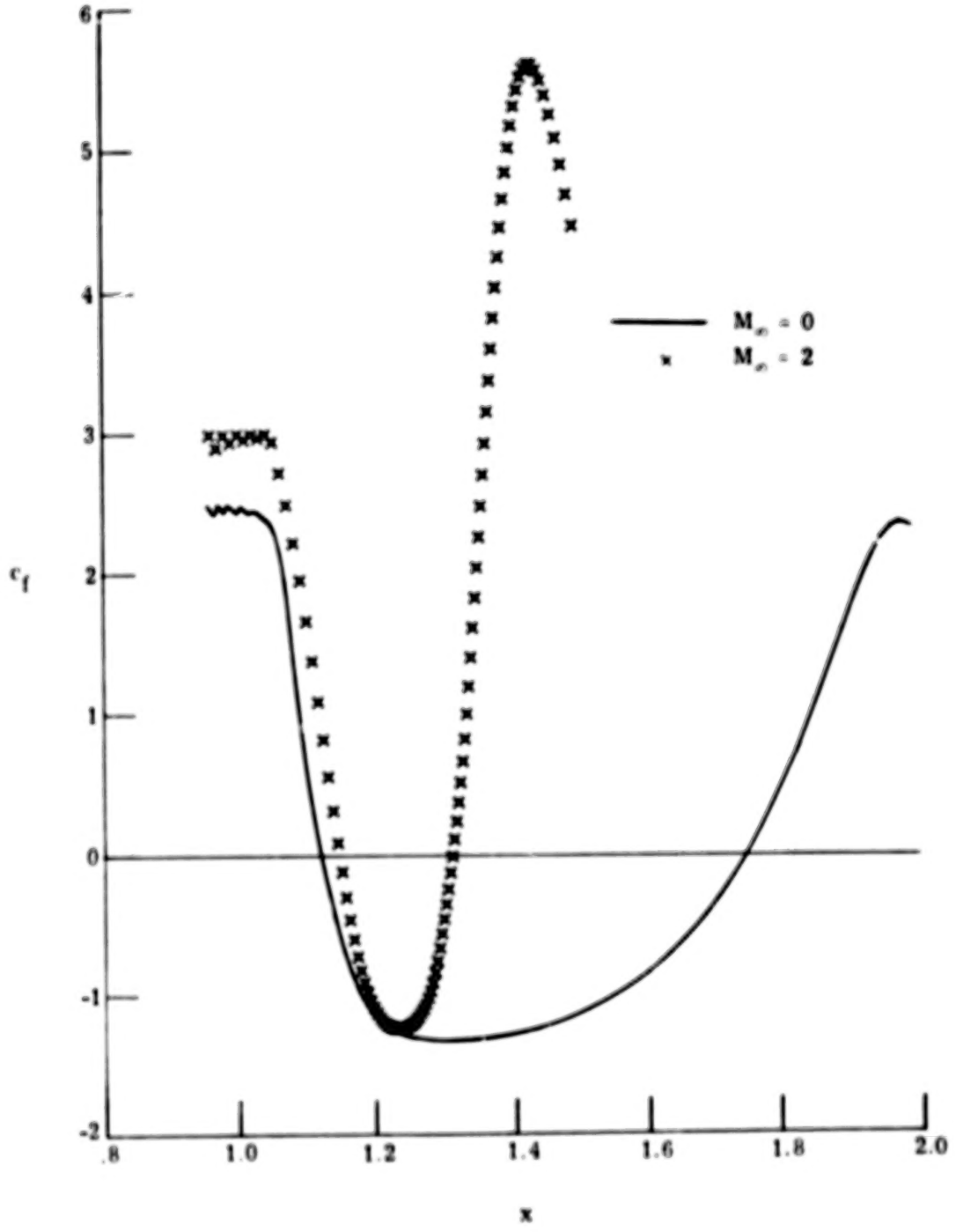

(c) Computed skin-friction distributions.

Figure 6.- Continued.

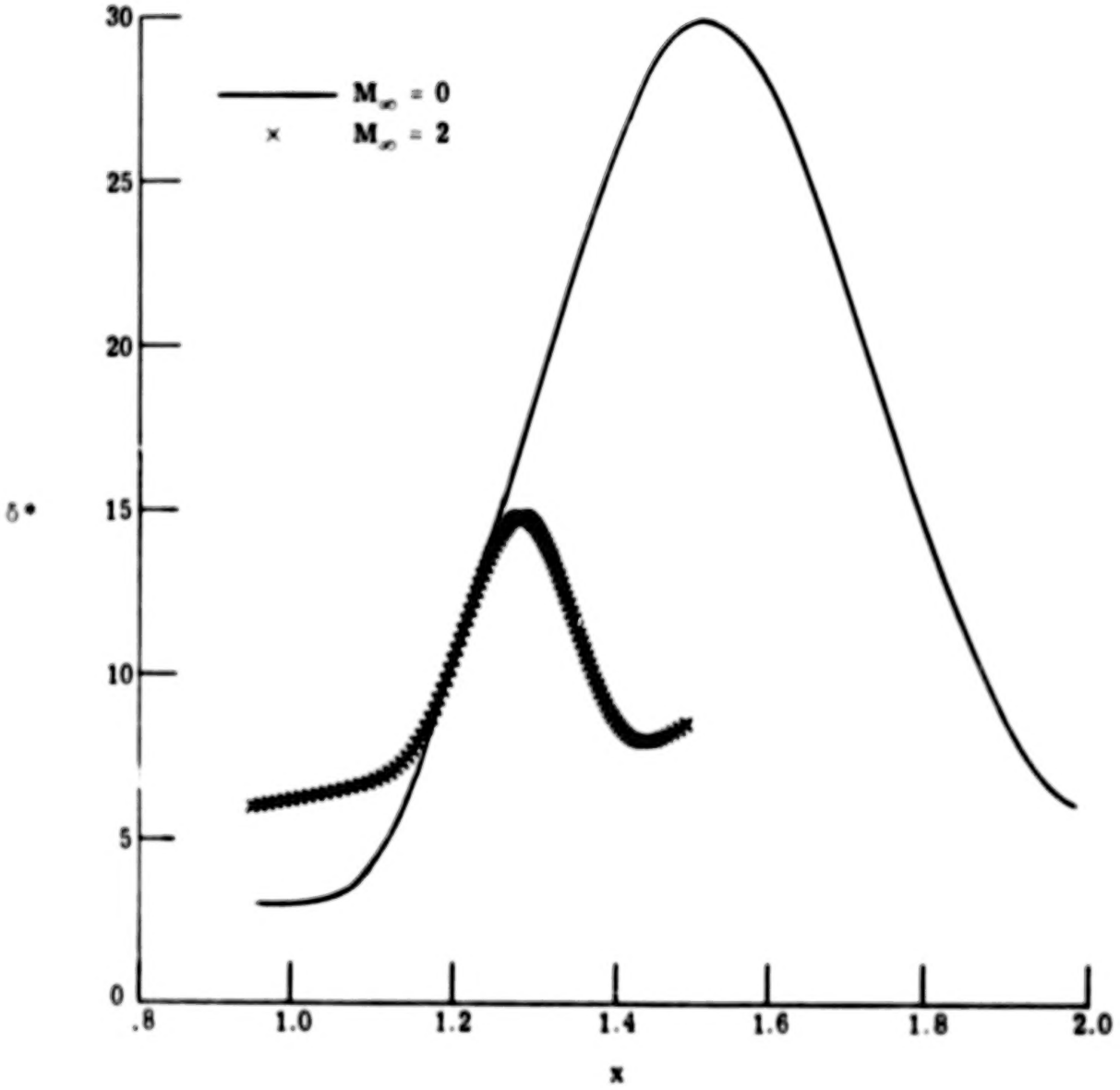

(d) Computed displacement-thickness distributions.

Figure 6.- Concluded.

1. Report No.	2. Government Accession No.	3. Recipient's Catalog No.
NASA TP-1208		

4. Title and Subtitle	5. Report Date
INVERSE BOUNDARY-LAYER THEORY AND COMPARISON WITH EXPERIMENT	September 1978
	6. Performing Organization Code
7. Author(s)	8. Performing Organization Report No.
James E. Carter	L-12190
	10. Work Unit No.
9. Performing Organization Name and Address	505-06-33-08
NASA Langley Research Center Hampton, VA 23665	11. Contract or Grant No.
	13. Type of Report and Period Covered
12. Sponsoring Agency Name and Address	Technical Paper
National Aeronautics and Space Administration Washington, DC 20546	14. Sponsoring Agency Code

15. Supplementary Notes

16. Abstract

Two new inverse boundary-layer computational procedures, which permit nonsingular solutions at separation and reattachment, are presented. In the first technique, which is for incompressible flow, the displacement thickness is prescribed; in the second technique, for compressible flow, a perturbation mass flow is the prescribed condition. The pressure is deduced implicitly along with the solution in each of these techniques. Laminar and turbulent computations, which are typical of separated flow, are presented and comparisons are made with experimental data. In both inverse procedures, finite-difference techniques are used along with Newton iteration. The resulting procedure is no more complicated than conventional boundary-layer computations. These separated boundary-layer techniques appear to be well suited for complete viscous-inviscid interaction computations.

17. Key Words (Suggested by Author(s))	18. Distribution Statement
Aerodynamics Boundary layers Separated flow Finite difference	Unclassified – Unlimited Subject Category 34

19. Security Classif. (of this report)	20. Security Classif. (of this page)	21. No. of Pages	22. Price*
Unclassified	Unclassified	53	$5.25

*For sale by the National Technical Information Service, Springfield, Virginia 22161

NASA-Langley, 1978

52